PNAS
www.pnas.org

Supplementary Information for

Self-adaptive and efficient propulsion of Ray sperms at different viscosities enabled by heterogeneous dual helixes

Panbing Wang[1†], M. A. R. Al Azad[2†], Xiong Yang[1], Paolo R. Martelli[3], Kam Yan Cheung[3], Jiahai Shi[2,4,5*], Yajing Shen[1,4*]

1 Department of Biomedical Engineering, City University of Hong Kong, Hong Kong, China.
2 Department of Biomedical Sciences, City University of Hong Kong, Hong Kong, China.
3 Ocean Park Corporation Hong Kong, Hong Kong, China
4 City University of Hong Kong Shen Zhen Research Institute, Shen Zhen, China.
5 Tung Biomedical Sciences Center, City University of Hong Kong, Hong Kong, China
†P. Wang and M. A. R. Al Azad contributed equally to this work.

*Correspondence to: Jiahai Shi and Yajing Shen
Email: jiahai.shi@cityu.edu.hk, yajishen@cityu.edu.hk

This PDF file includes:

Figures S1 to S29
Tables S1 to S16
Legends for Movies S1 to S5
Code availability
SI reference

Other supplementary materials for this manuscript include the following:

Movies S1 to S5

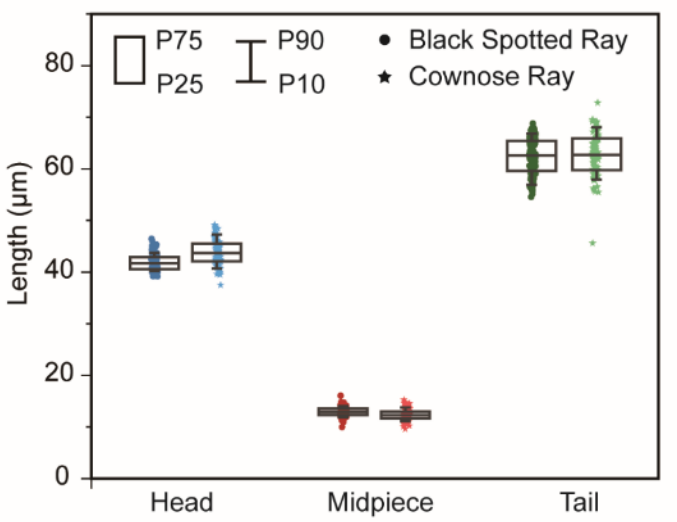

Fig. S1. Length of the head, midpiece and tail of Ray sperms (n=100). The length of the head, midpiece and tail of the Black Spotted Ray are 41.93±0.15 μm, 13.01±0.09 μm, and 62.43±0.35 μm, respectively. The length of the head, midpiece and tail of the Cownose Ray are 43.87±0.25 μm, 12.4±0.11 μm, and 62.8±0.42 μm, respectively.

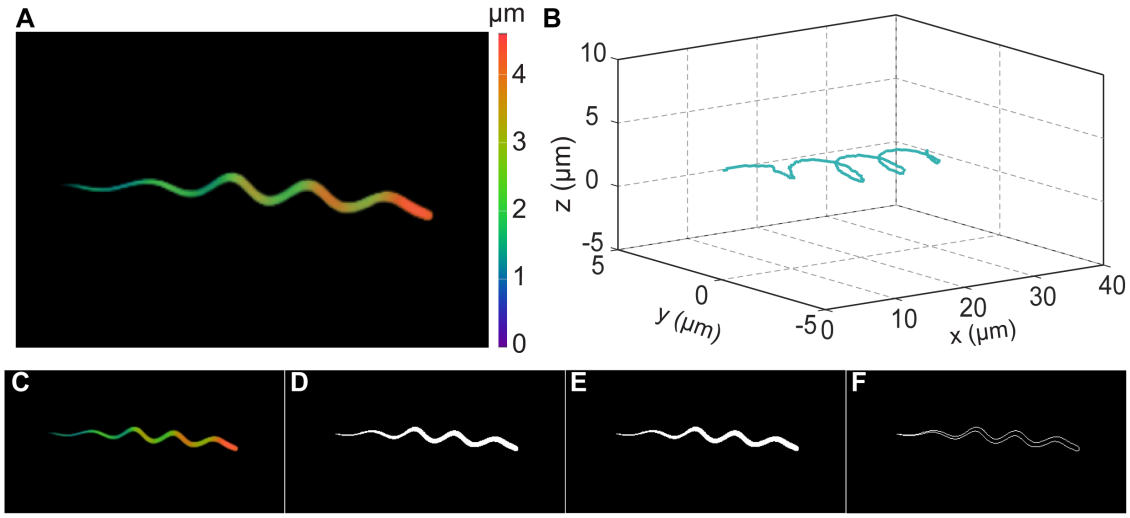

Fig. S2. Confocal images of the Ray sperm head. (A). The Confocal image of the sperm head. The height of each point is illustrated by the color bar. (B). The centerline of the sperm head after image processing. (C-F). Image processing results: (C) Region of interest, (D). thresholding, (E). maximum connected domain, (F) edge detection.

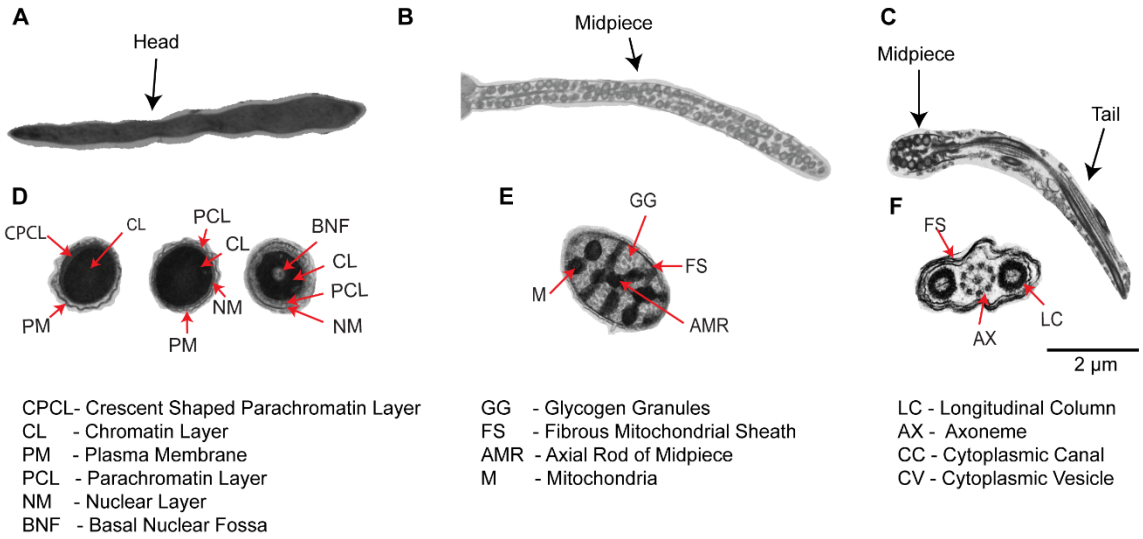

Fig. S3. TEM images of the Ray sperm. A-C. Longitudinal sections of the head, midpiece, and tail. D-F. Cross sections of the head, midpiece, and tail.

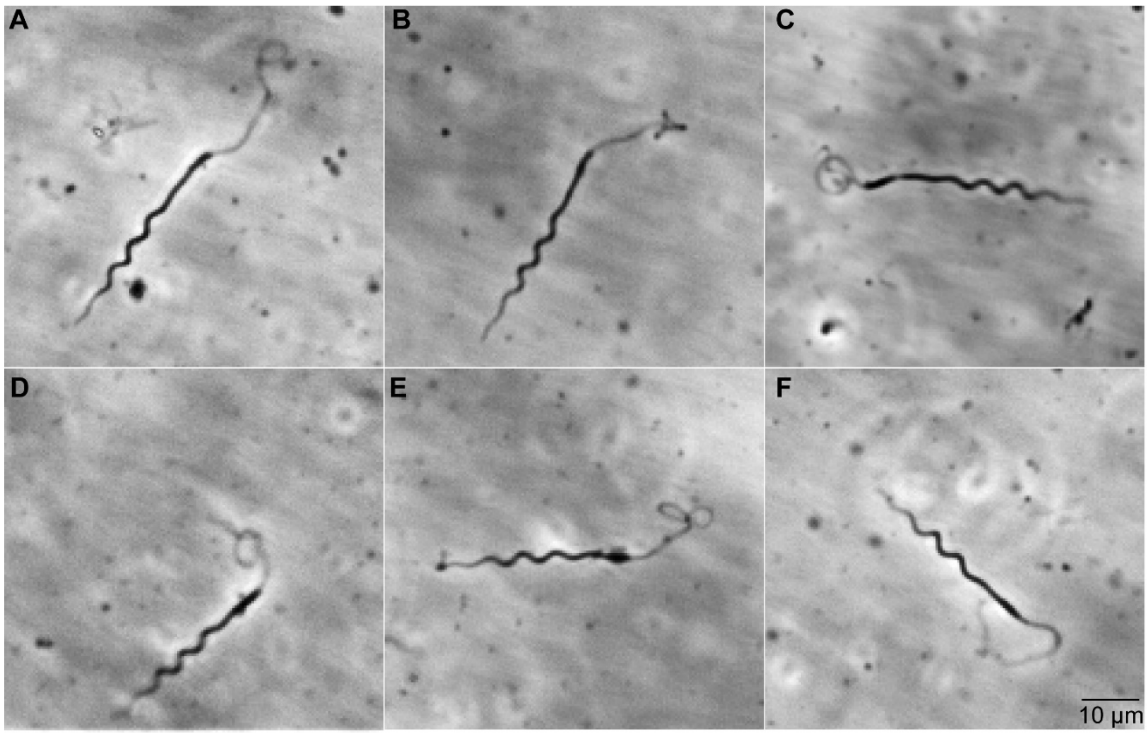

Fig. S4. Shape of the tail in different status. The tail of the sperm exhibits various shapes when the sperm is blocked or not in the normal condition.

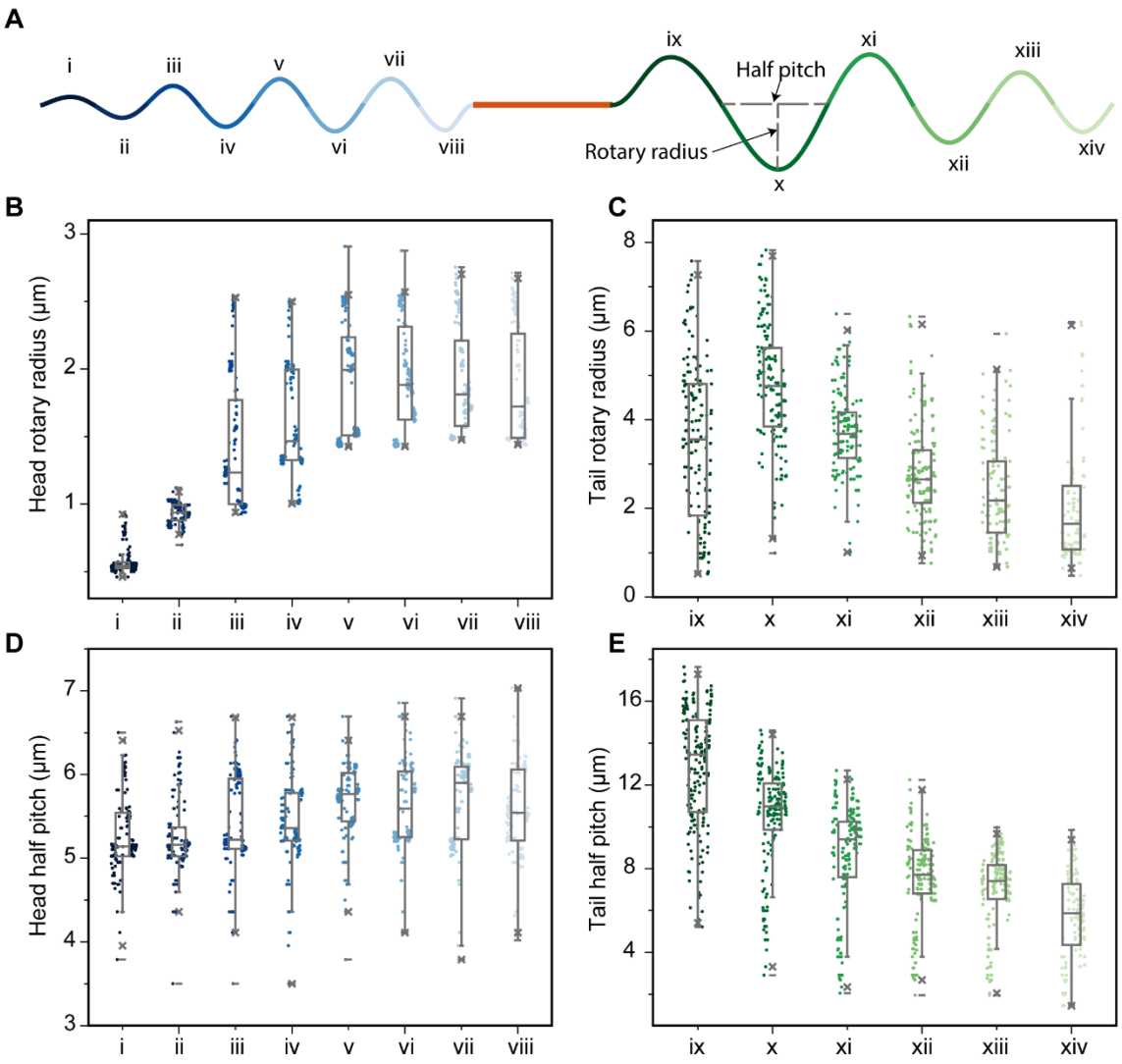

Fig. S5. Helical shape illustration of Ray sperms. A Definition of the two shape parameters: amplitude A_m and half of the pitch H_p to illustrate the helical shape of head and tail. The amplitude represents the rotational amplitude when the head or tail rotates. The half of the pitch means the distance on the body axis between two half circles. Amplitude (B-C) and half of the pitch (D-E) measurements of the sperm head and tail. The distribution of head parameters are more concentrated compared with that of tail, which shows the variational softness of the total body.

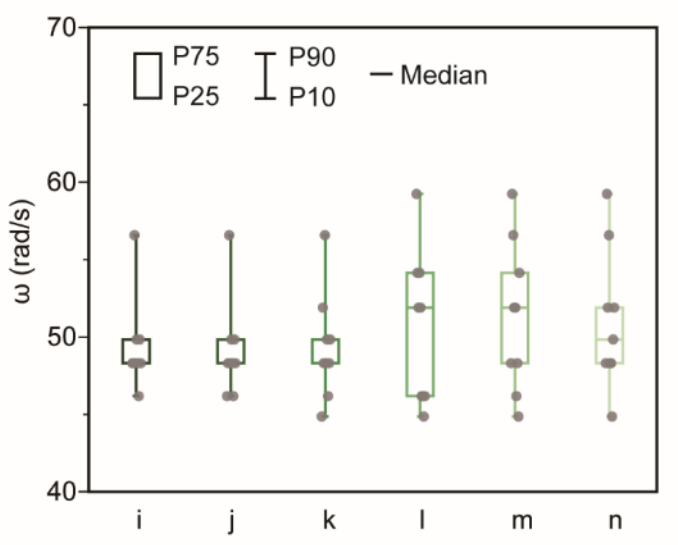

Fig. S6. Rotational speed of the 6 half circles on the tail. The average of the rotational speed on the 6 half circles are 49.3 rad/s, 49.1 rad/s, 49.4 rad/s, 50.5 rad/s, 51.3 rad/s, and 51.0 rad/s with the maximum standard error of 4.9 rad/s (n=9).

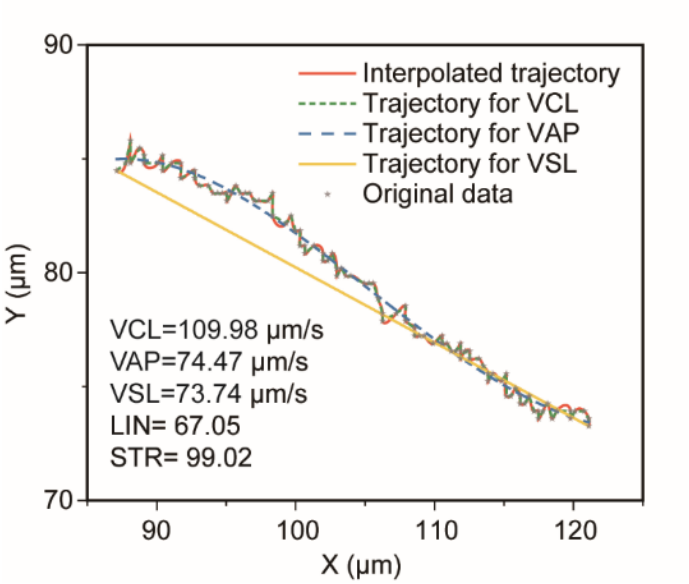

Fig. S7. Trajectory and motility parameters of the representative Ray sperm. The original points, interpolated trajectory, curve trajectory, average trajectory, and the straight trajectory are displayed (data points > 190). The corresponding curvilinear velocity (VCL), average path velocity (VAP), and straight-line velocity (VSL) were 109.98 μm/s, 74.47 μm/s, and 73.74 μm/s, respectively. The Linearity and straightness of the trajectory were 67.05% and 99.02%, respectively.

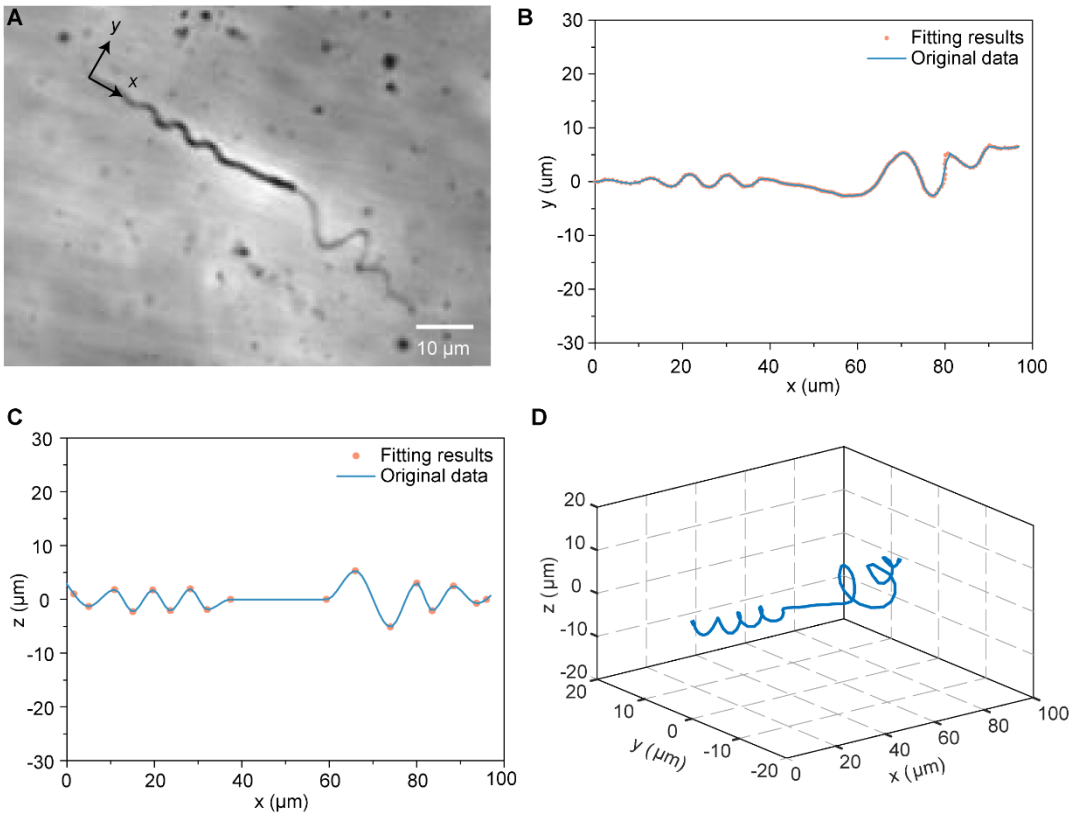

Fig. S8. 3D reconstruction results of the sperm. (A) The original image of a sperm, (B) the fitting results on the X-Y plane, (C) fitting results on the X-Z plane, (D) the 3D reconstruction results.

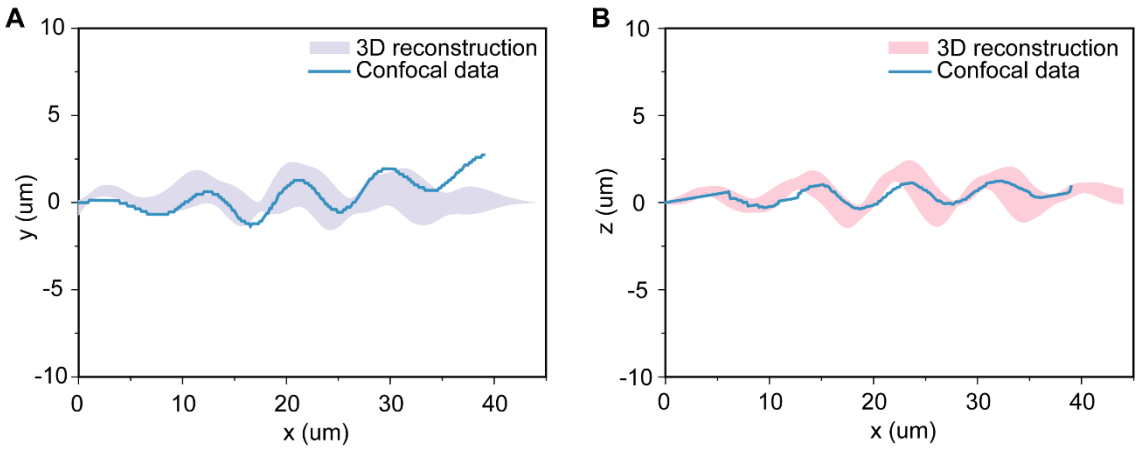

Fig. S9. Comparison of the 3D reconstruction based on the optical image and the confocal image. (A). Reconstruction data on the X-Y plane, (B). reconstruction data on the X-Z plane (n=5).

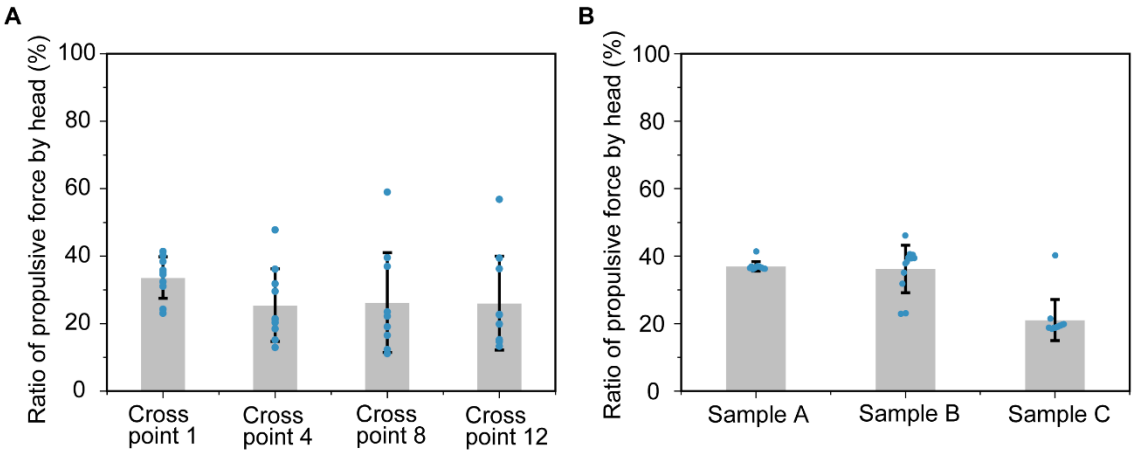

Fig. S10. Calculation results of the propulsive force based on the Regularized Stokeslet Method. (A). The ratio of propulsive force produced by the head with different numbers of points per cross-section (n=10). (B). The ratio of propulsive force produced by the head of three samples with the number of points per cross-section from 1 to 12.

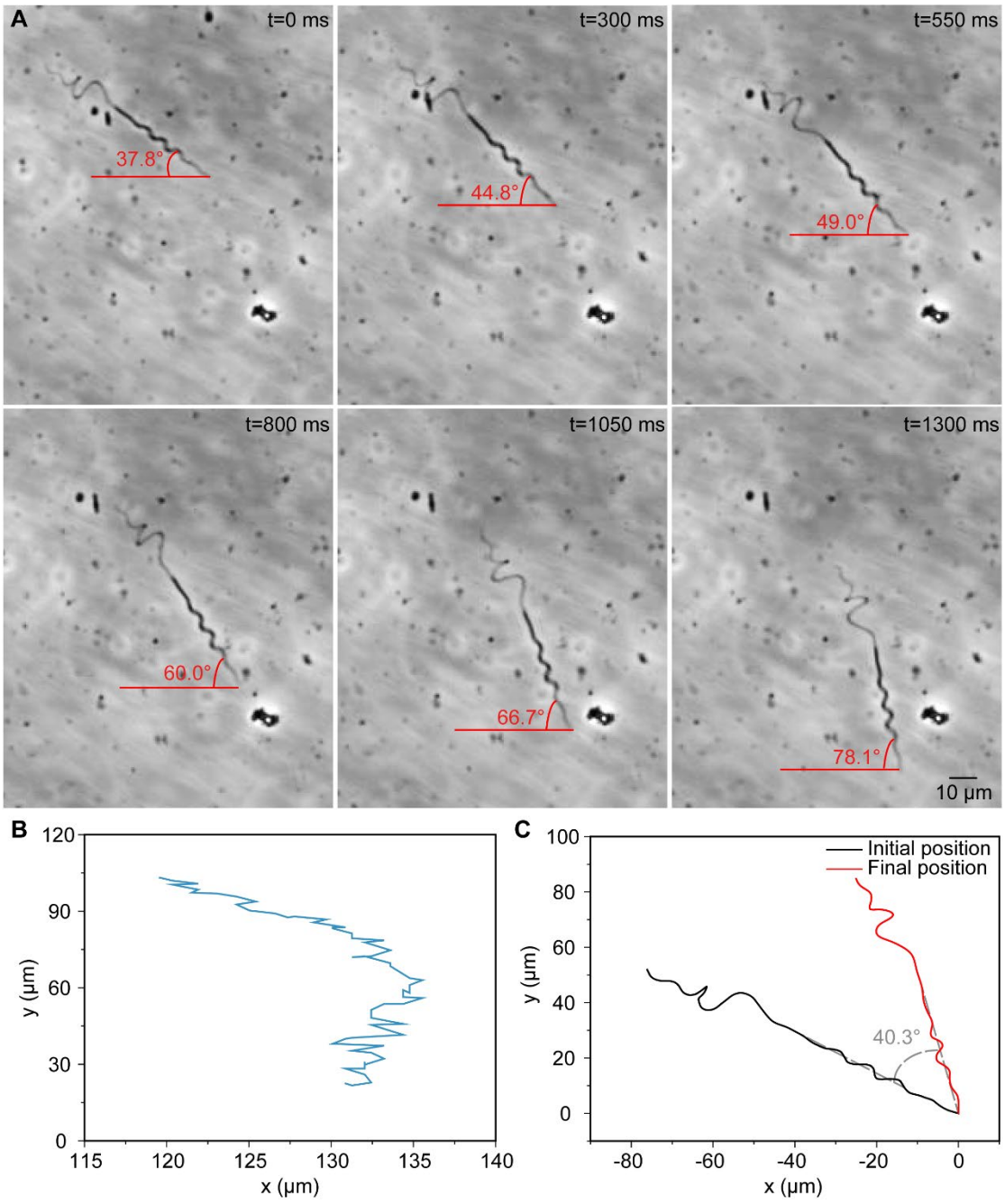

Fig. S11. Turning motion of a sperm. The sperm moves in the right direction during the forward motion. A. Image sequences, B. Trajectories, C. Morphologies at the initial and final time.

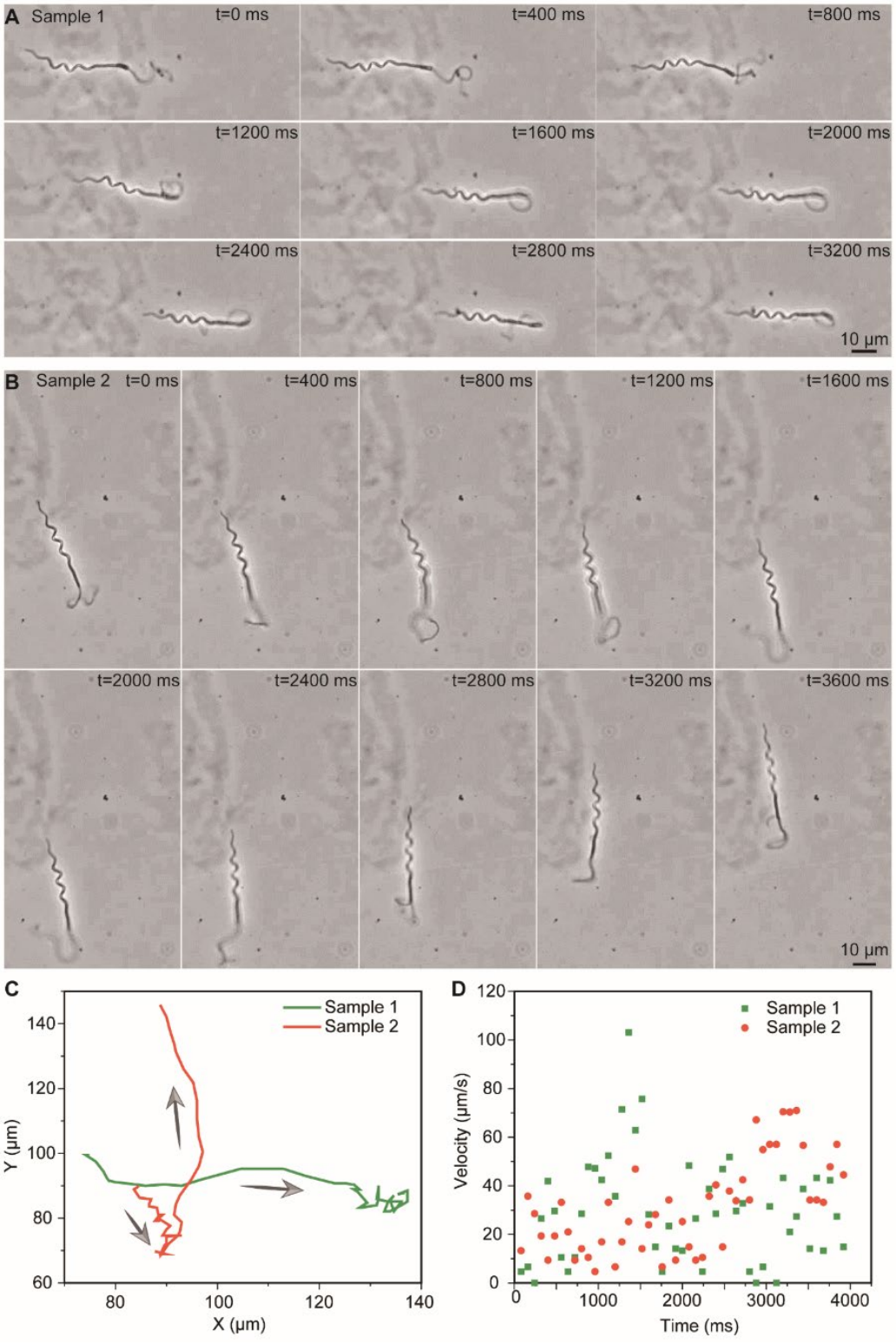

Fig. S12. Bi-directional motions of sperms when encountering obstacles. (A-B) image sequences of sperms encountering obstacles and the corresponding trajectories (C) and velocities (D). The velocity data is calculated from the trajectories in C. For the sample 1, it moved backward

to stay away from the obstacle. The sperm in B first moved backward to avoid the obstacle, then moved forward.

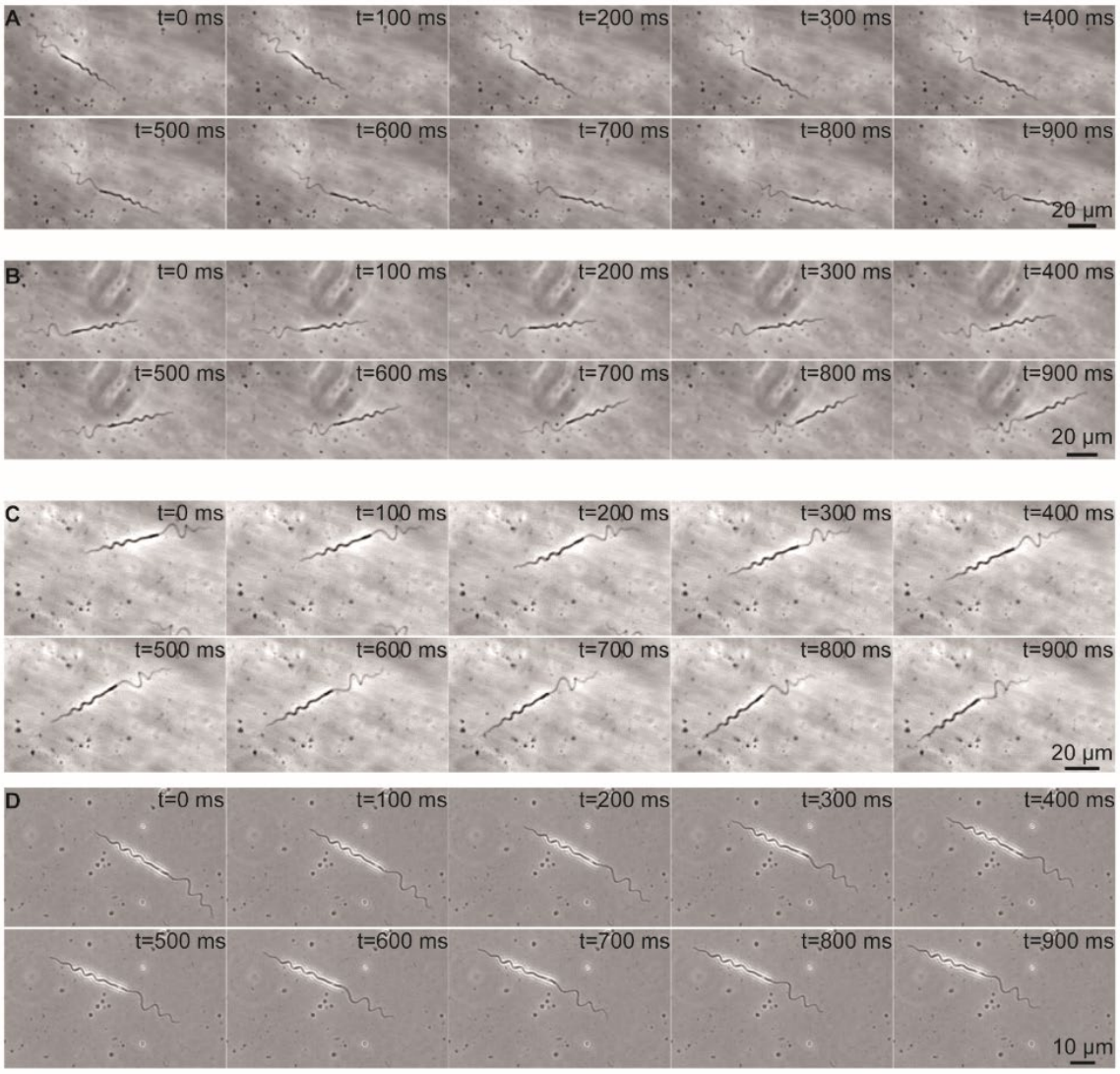

Fig. S13. Image sequences of the forward motion of sperms. The four sperms moved forward with the rotation of both head and tail, corresponding to the sample 1-4 in Fig. 4(B-C).

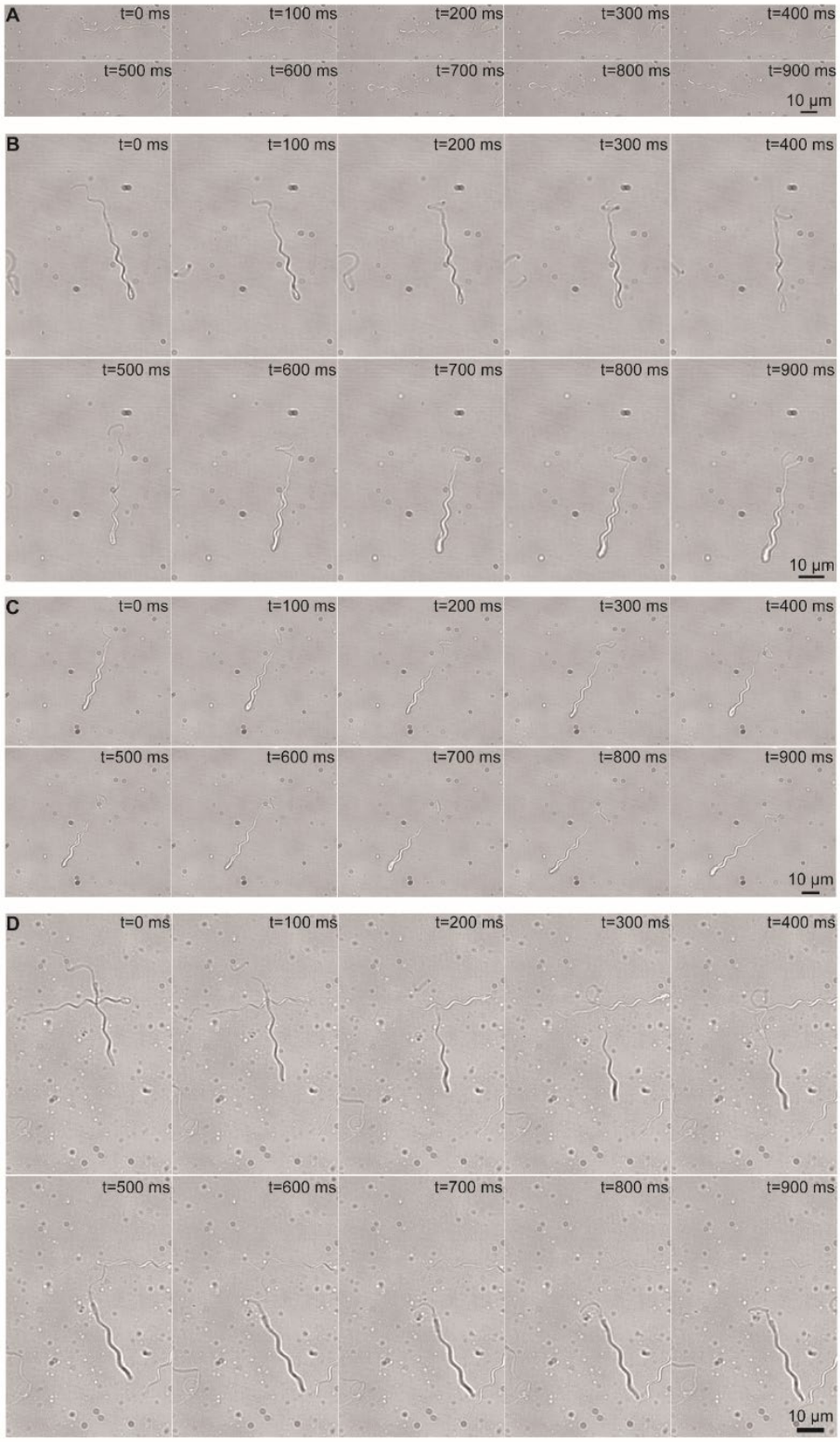

Fig. S14. Image sequences of the backward motion of sperms. The four sperms moved backward totally, corresponding to the sample 5-8 in Fig. 4(B-C).

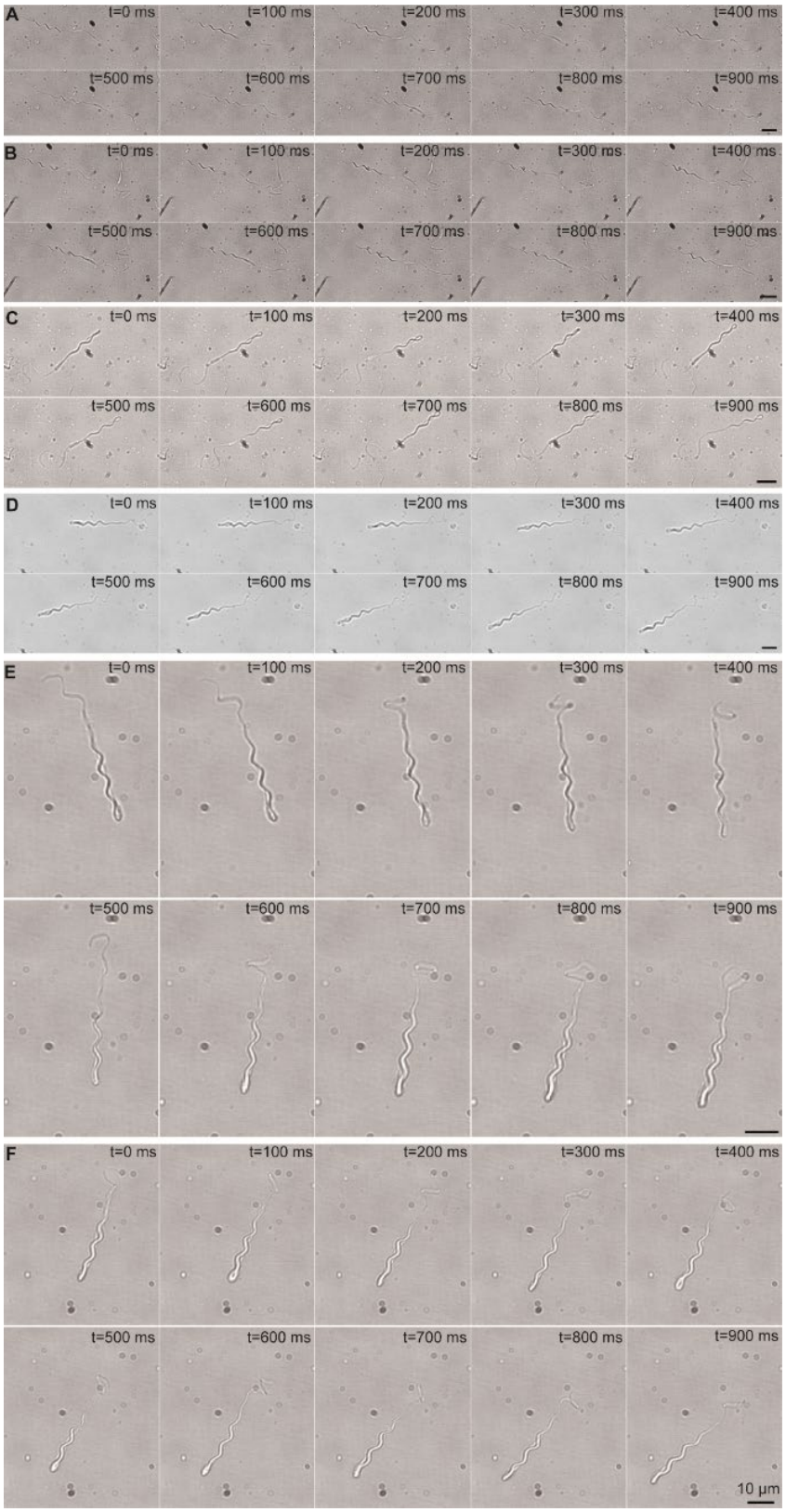

Fig. S15. Image sequences of the backward motion of sperms. The six sperms moved backward totally, corresponding to the sample 1-6 in Fig. 4E.

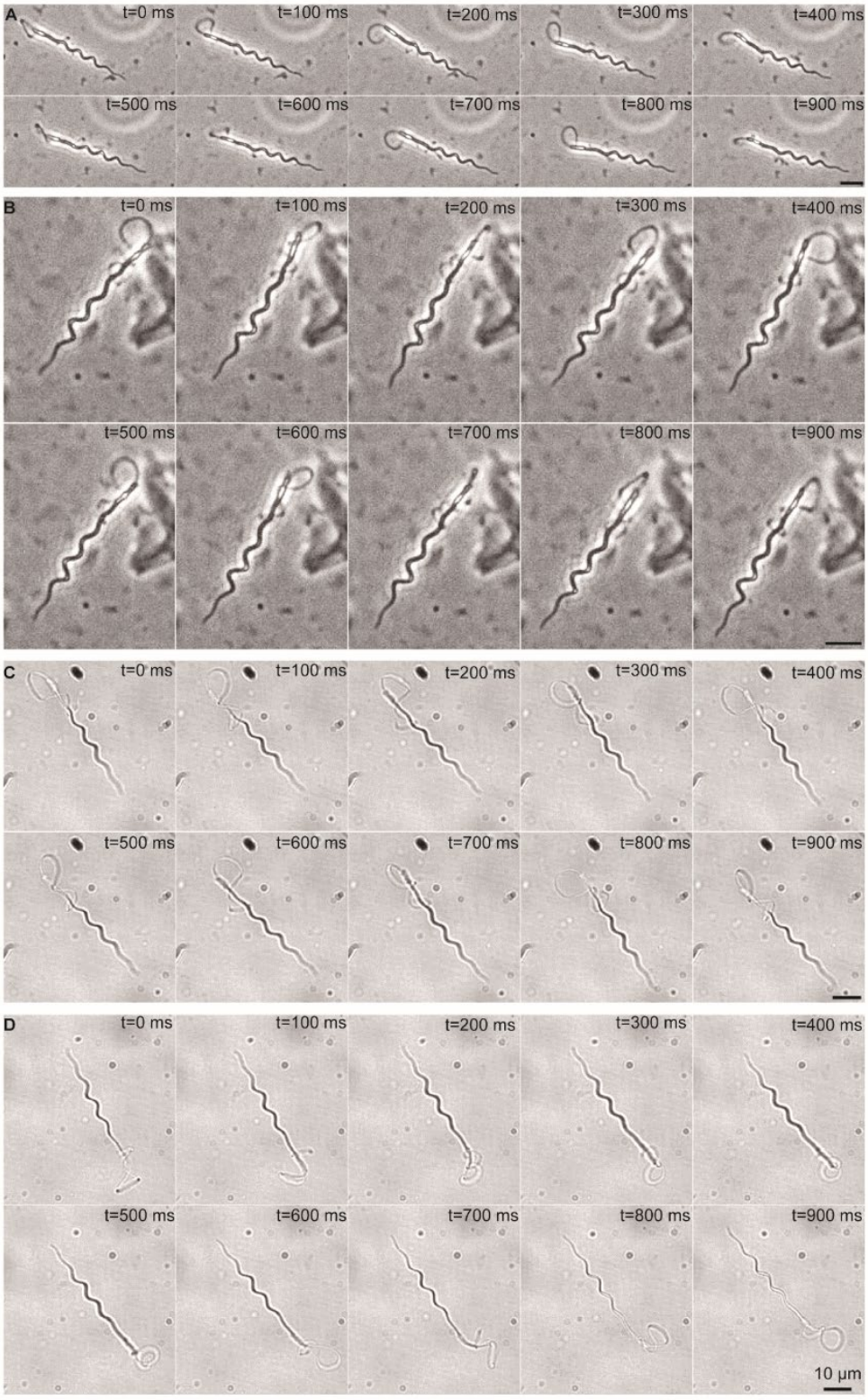

Fig. S16. Image sequences of sperms moving in viscous solution i. The sperms moved in the viscous solution i with the twinning tail and the helical head, which provided the propulsive force for the movement. The four sperms are corresponding to the sample 5-8 in Fig. 5E.

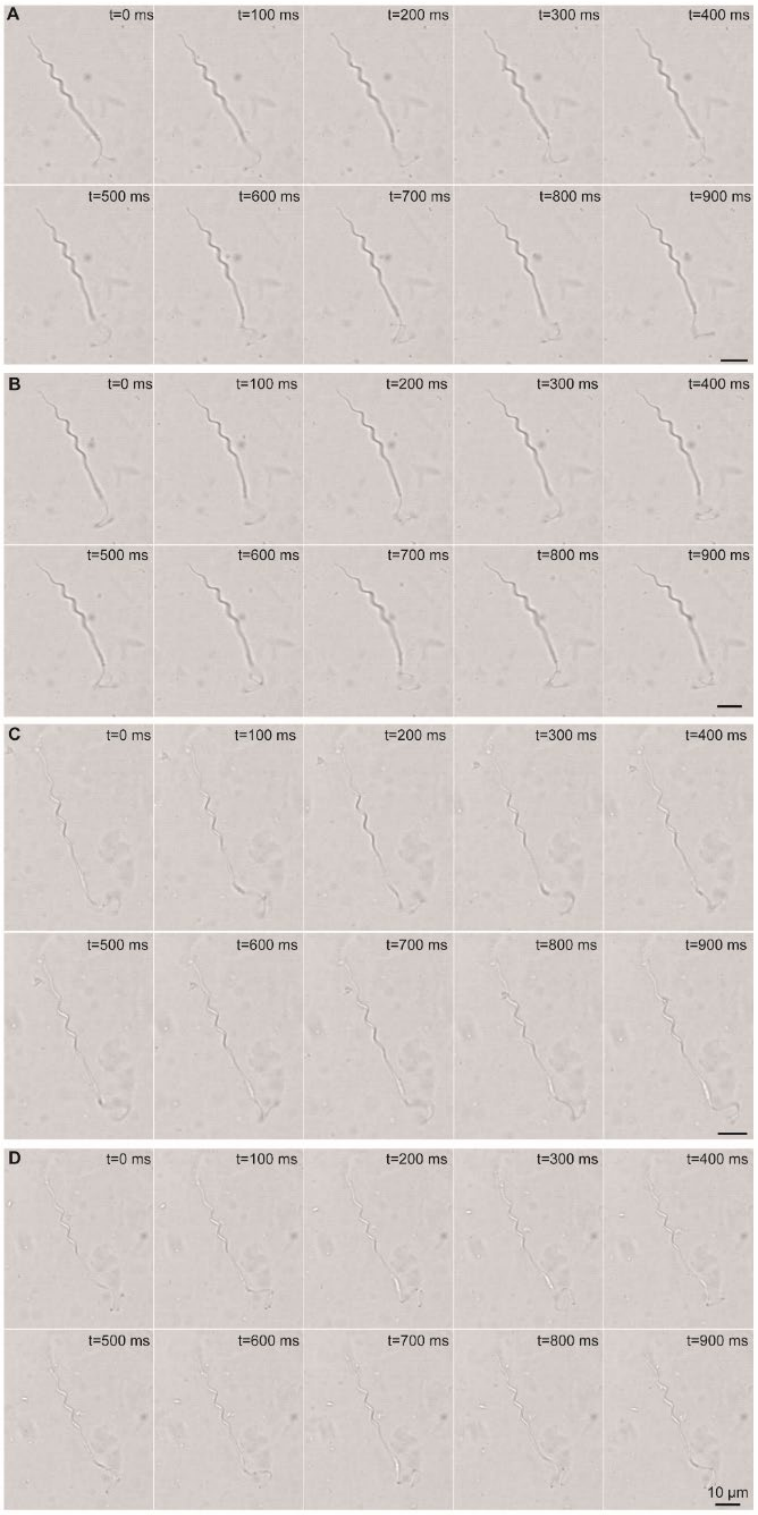

Fig. S17. Image sequences of sperms moving in viscous solution ii. The sperms moved in the viscous solution ii with the twinning tail and the helical head, which provided the propulsive force for the movement. The four sperms are corresponding to the sample 9-12 in Fig. 5E.

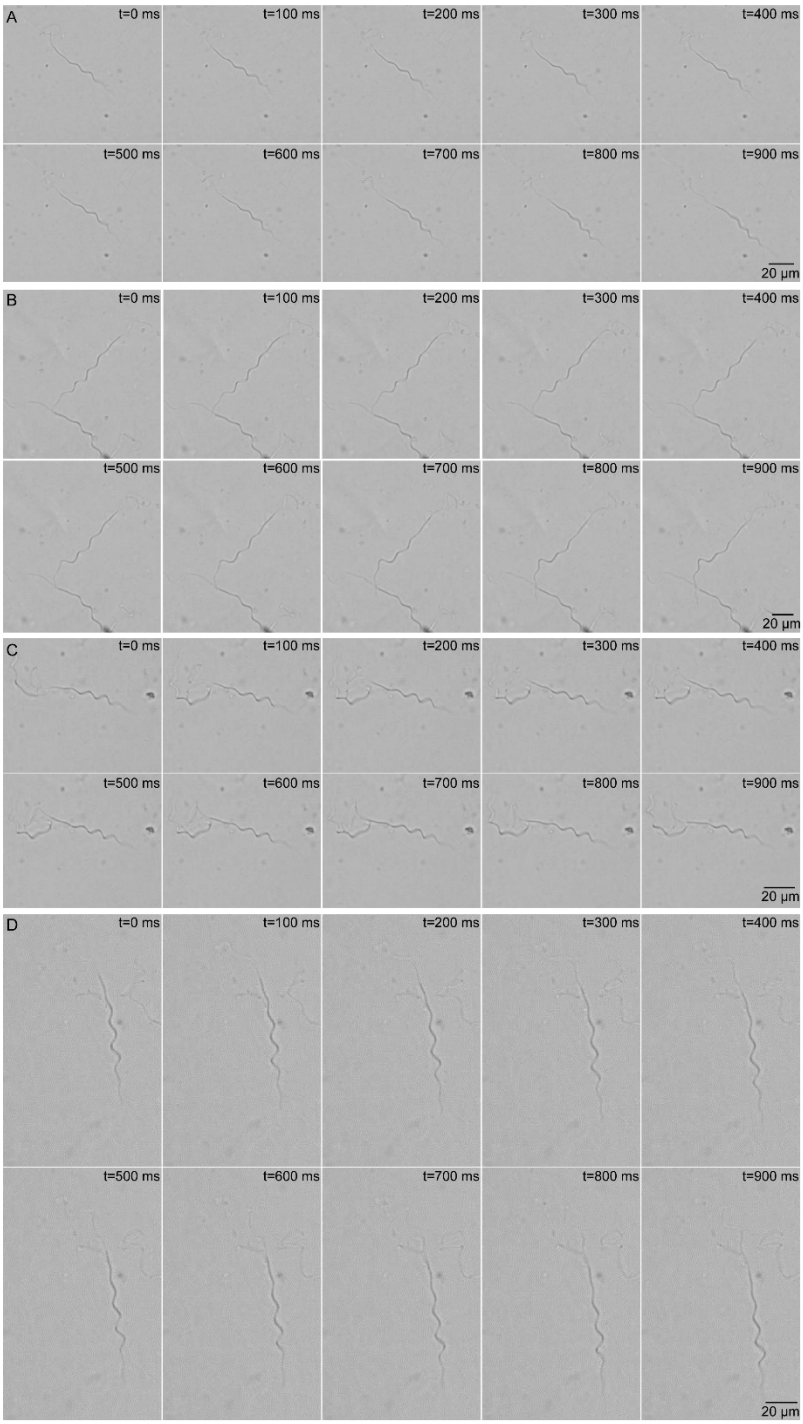

Fig. S18. Image sequences of sperms moving in viscous solution iii. The sperms moved in the viscous solution iii with the twinning tail and the helical head, which provided the propulsive force for the movement. The four sperms are corresponding to the sample 13-16 in Fig. 5E.

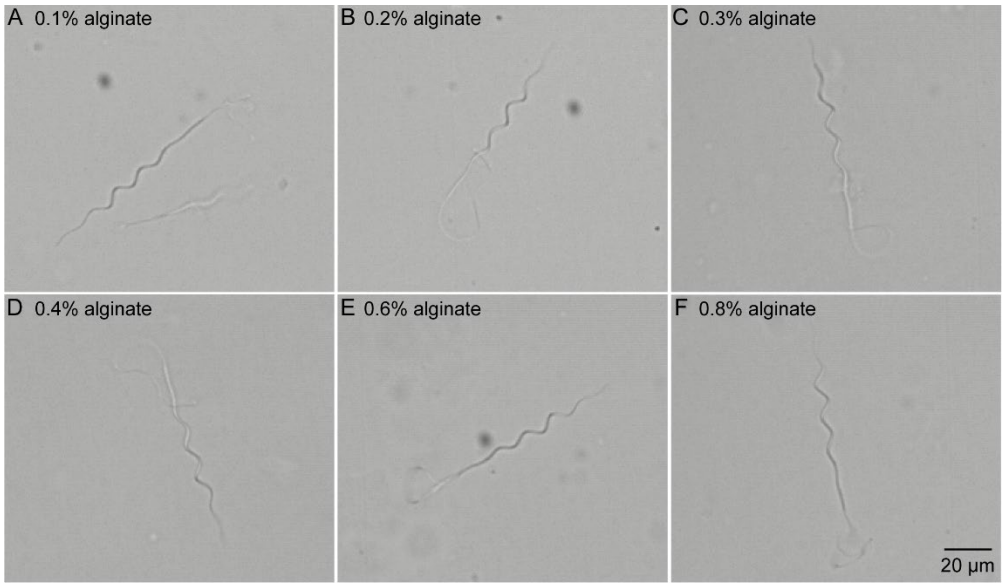

Fig. S19. Image sequences of sperms moving in viscous solutions (0.1%, 0.2%, 0.3%, 0.4%, 0.6, and 0.8% alginate).

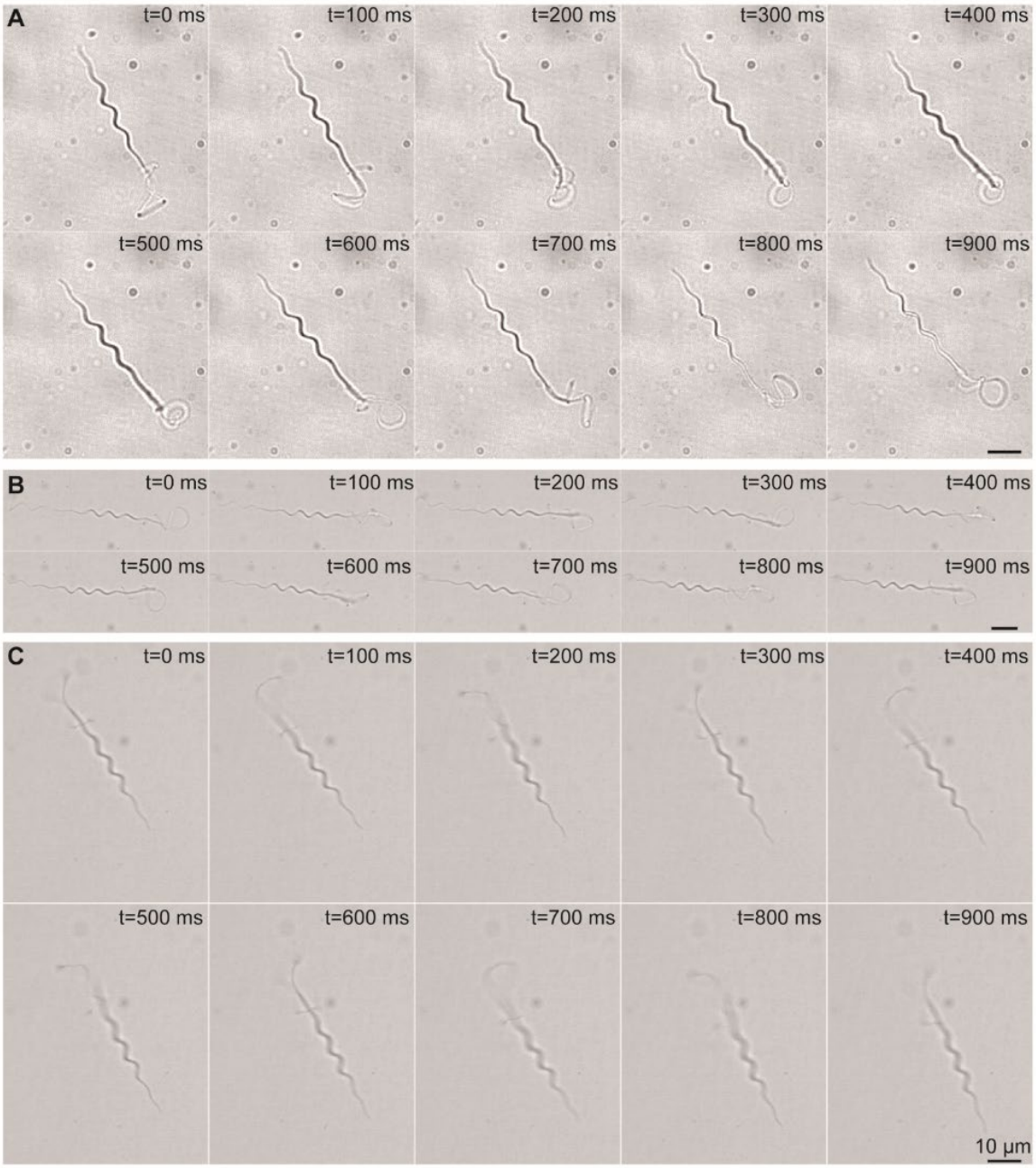

Fig. S20. Image sequences of sperms moving in viscous solution i for speed fitting. The sperms are corresponding to the sample 1-3 in viscous solution i in Fig. 5H.

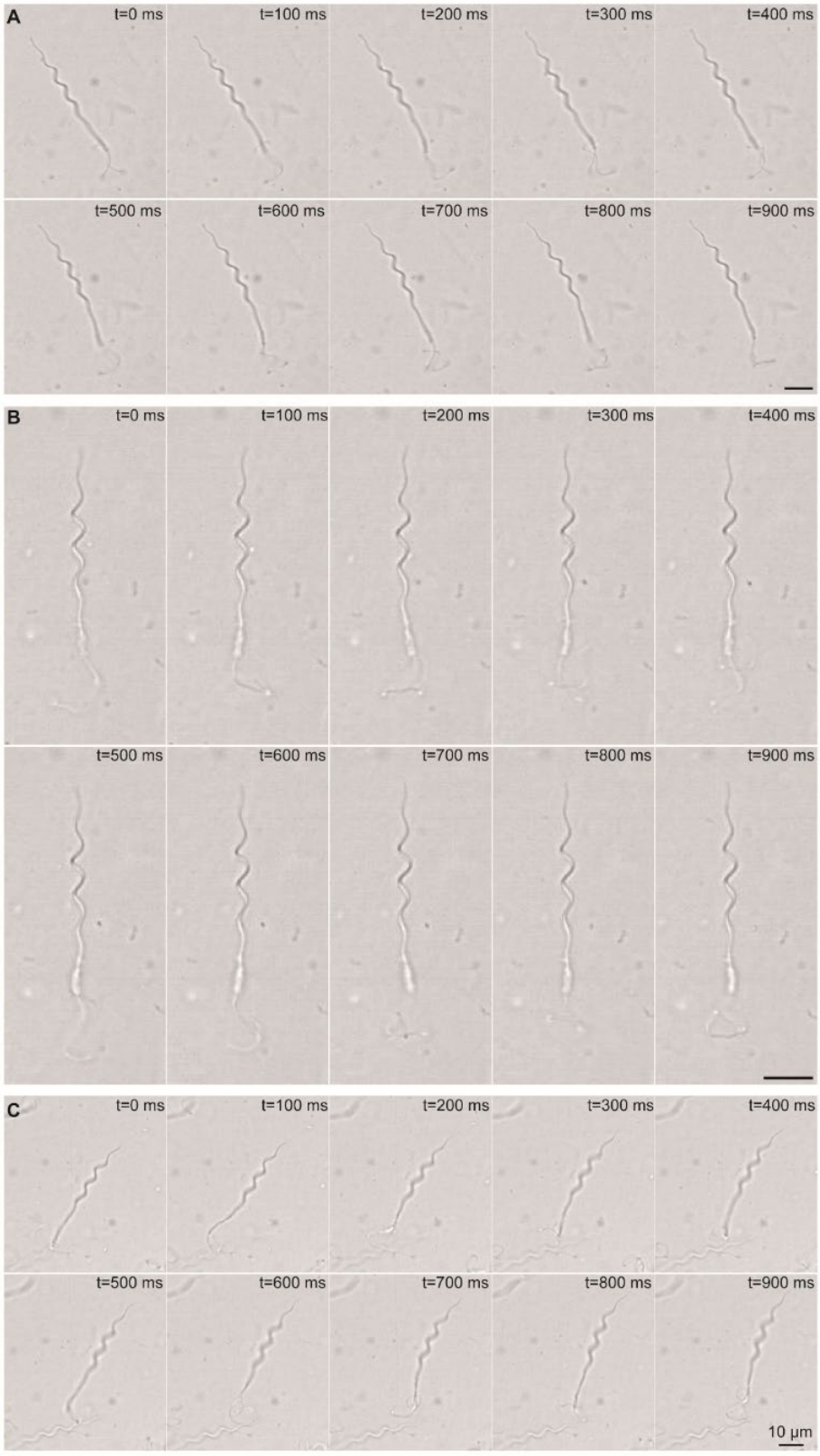

Fig. S21. Image sequences of sperms moving in viscous solution ii for speed fitting. The sperms are corresponding to the sample 1-3 in viscous solution ii in Fig. 5H.

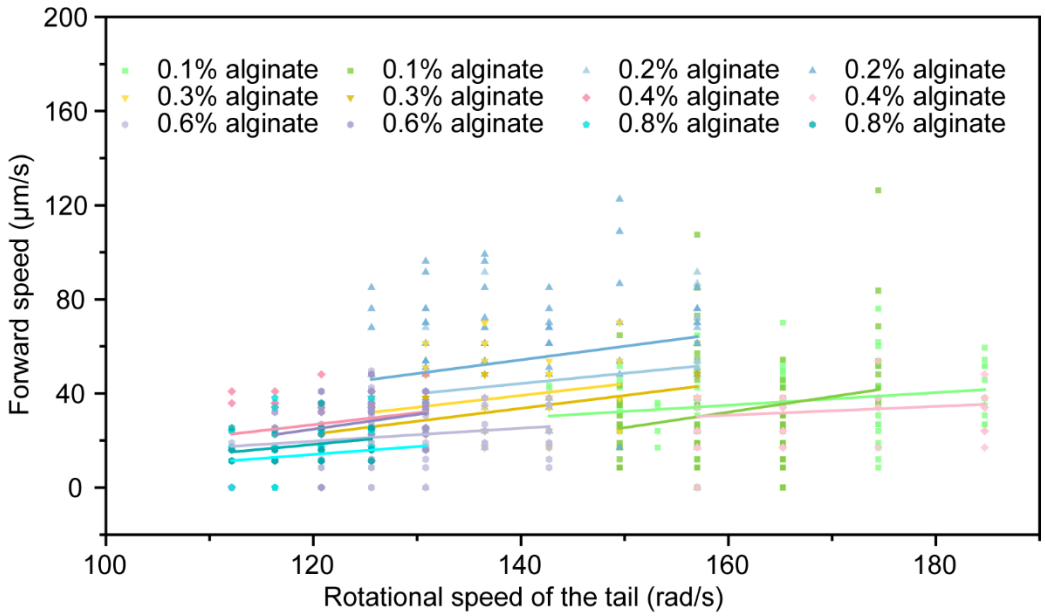

Fig. S22. Relationship between the rotational speed of the tail and the forward speed in various viscous solutions.

Fig. S23. Image sequences of distance between the slide and the coverslip.

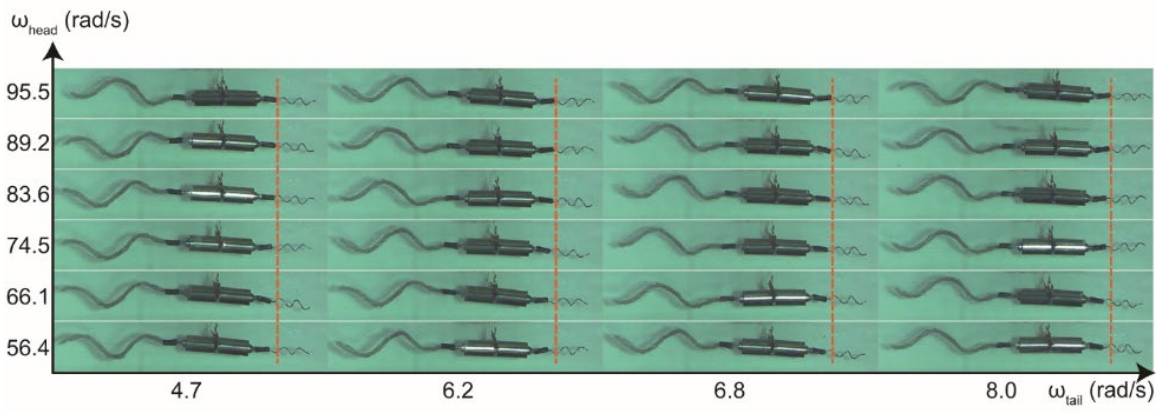

Fig. S24. Images of the robot moving with increasing rotational speeds of head and tail after moving 4 seconds. With the increase of rotational speeds of head and tail, the robot moved longer after 4 seconds, indicating the rise of the forward speed along with the rotational speeds.

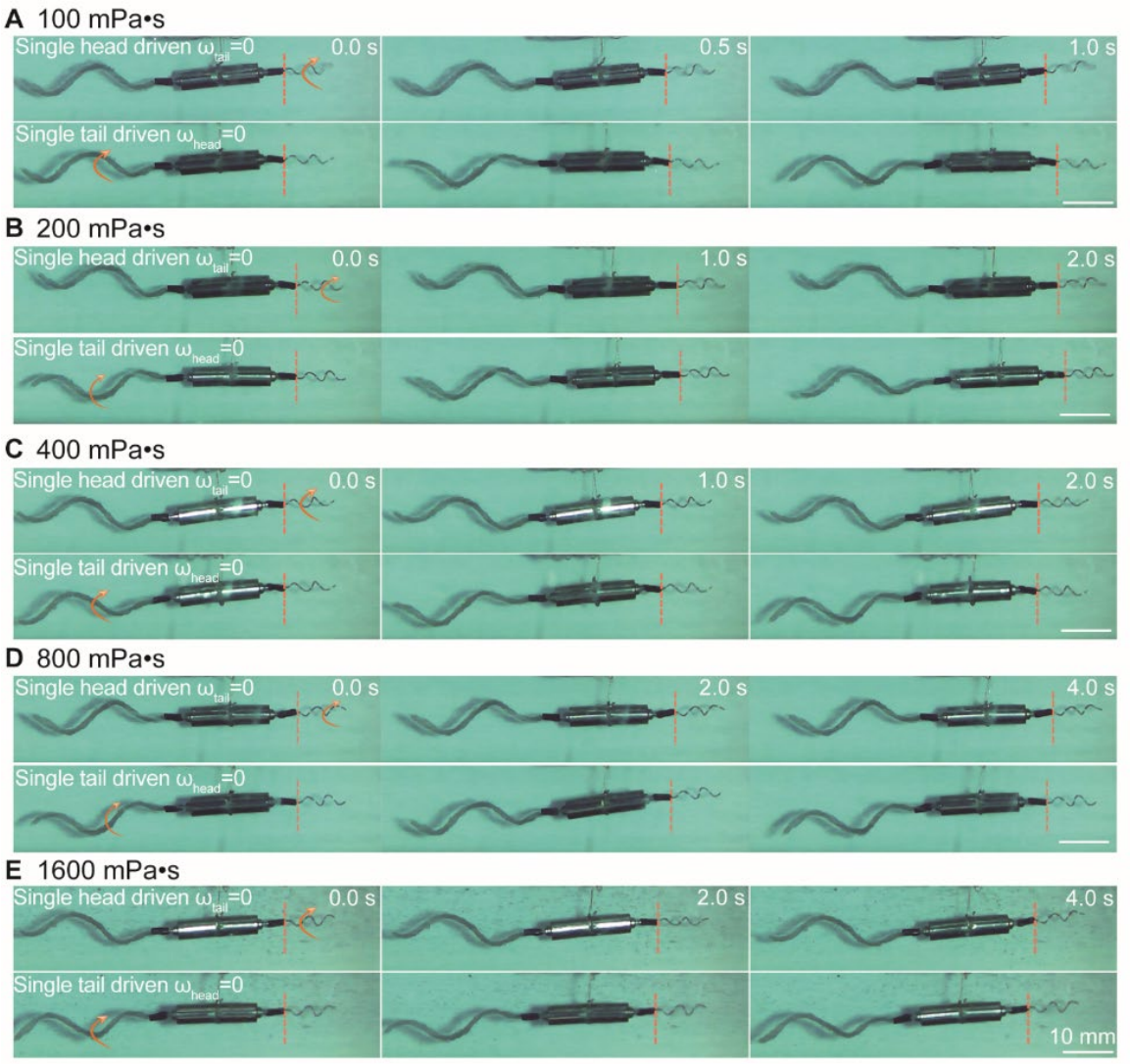

Fig. S25. Image sequences of the robot with single drive. The robot was driven by single helical head or tail with same power input in different viscous solutions: 100 mPa·s (A), 200 mPa·s (B), 400 mPa·s (C), 800 mPa·s (D), and 1600 mPa·s (E). In the dilute solution, the robot with tail driven moved faster than that with head driven. In contrast, the robot driven by the helical head performed better in the highly viscous solution.

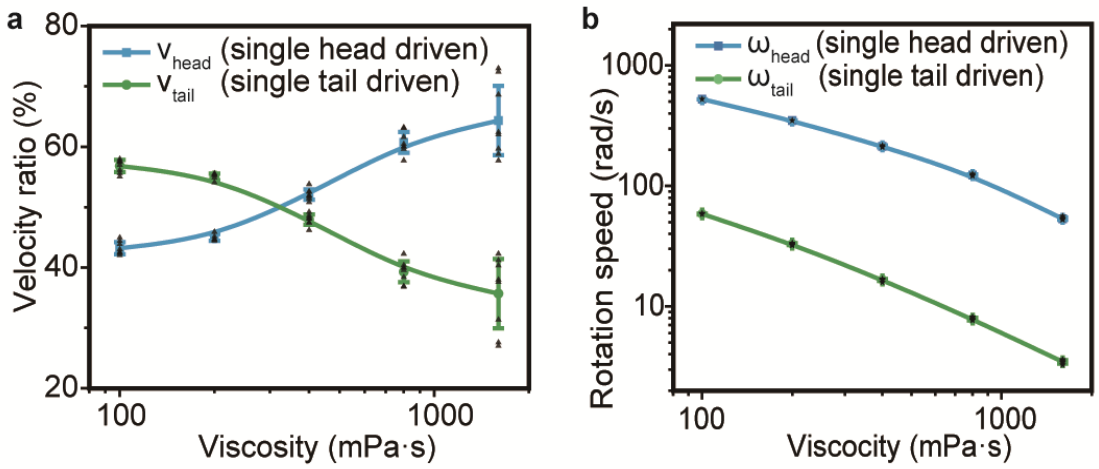

Fig. S26. Forward speed (a) and Rotational speeds (b) of the robot with a single drive under the same power input (n=3). The two rotational speeds decreased along with the growth of the viscosity, and the rotational speed of tail first decreased below 10 rad/s while the head remains 54.5 rad/s in the 1600 mPa·s solution. The velocity ratio in f represents the velocity driven by head (v_{head}) or tail (v_{tail}) dividing the sum of those two velocities ($v_{head} + v_{tail}$), illustrating the propulsive efficiency of the head is higher in the viscous solution but the tail dominates in the dilute solution.

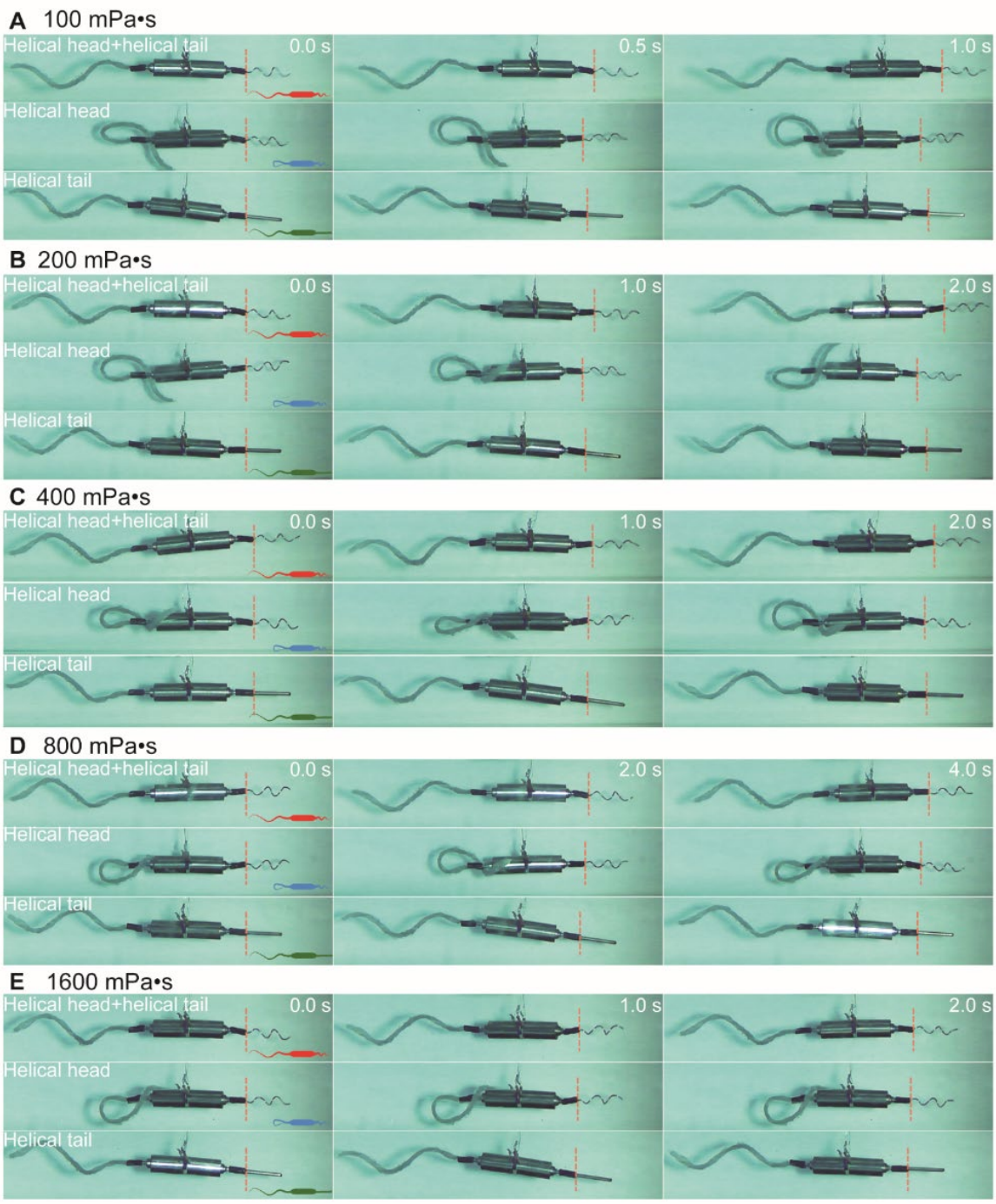

Fig. S27. Image sequences of the robot with dual or single helical structure. The robot was driven by dual or single helical structure with same power input in different viscous solutions: 100 mPa·s (A), 200 mPa·s (B), 400 mPa·s (C), 800 mPa·s (D), and 1600 mPa·s (E).

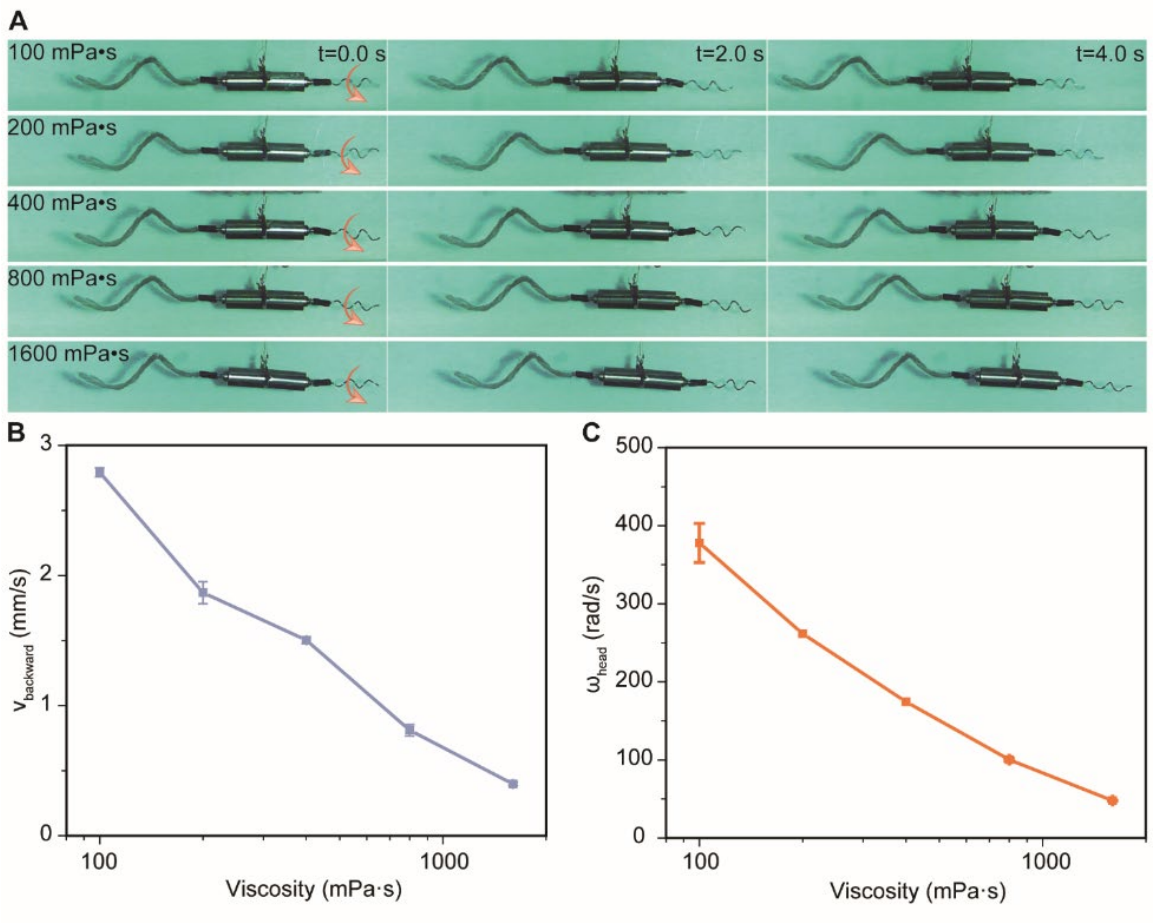

Fig. S28. Backward motion of the bio-inspired robot. The image sequences (A), corresponding backward velocity (B), and rotational speed of head (C) of the bio-inspired robot. The robot can move backward in various viscous solutions while the head made the dominate contribution of the propulsive force.

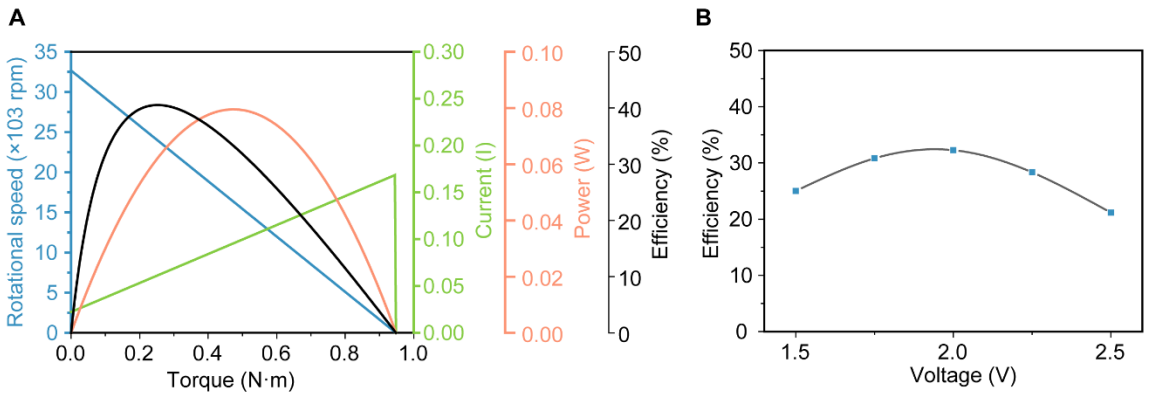

Fig. S29. Mechanical behavior of the motor. (A) Changing curves of the rotational speed (blue), current (green), power (orange), and efficiency (black) of the motor (voltage=2.5 V). (B) Efficiency of the motor under the fixed power (0.075 W).

Table S1. Chemicals Used for Experiments

SL No	Chemical Name	Company Name	Catalogue No
1	NaCl	Acros Organics	AC207790010
2	KCl	Merck, Germany	104936
3	$CaCl_2$	VWR	11J210025
4	Na_2So4	Merck	7757-82-6
5	$NaHCO_3$	Sigma	144-55-8
6	Na_2HPO_4	Fisher Scientific	7558-79-4
7	Glucose	Alfa Aesar	50-99-7
8	Urea	Uni-Chem	57-13-6
9	TMANO	TCI Chemicals	1184-78-7
10	Sodium Alginate	Acros Organics, USA	AC177772500
11	Osmium (VIII) Oxide	ALFA ASER	20816-12-0
12	Paraformaldehyde	Merck	104005
13	Glutaraldehyde	Merck	340855
14	Acetone	Thermo Fisher	67-64-1
15	Ethanol	Merc	100983
16	Hoechst 33342	Sigma Aldrich	40825
17	Mitotracker Red CM-H2XRos	Oregon, USA	1837174

Table S2. Length data of sperms

Species	Head (μm)	Midpiece (μm)	Tail (μm)	Ratio
Rooster[1]	13.84	4.13	73.39	3.4:1:17.8
Esox Lucius[2]	1.32	1.17	32.0	1.1:1:27.4
Siberian sturgeon[3]	5.92	1.09	44.75	5.4:1:41.1
Beluga[4]	6.96	2.1	42.21	3.3:1:20.1
Ray	**42.9**	**12.7**	**62.6**	**3.4:1:4.9**

Table S3 Significance test of the regression of the propulsive ratio of head.

	F-value	P-value	$F_{0.05}$	$F_{0.01}$	Effect size (r)	95% confidence interval	T-value	P-value	$T_{0.05}$	$T_{0.01}$
Regression	828.66	P<0.001	2.63	3.83	0.93	—	——	——	—	—
b_1=0.11	——	——	—	—	—	[0.11, 0.12]	33.90	P<0.001	1.97	2.59
b_2=-0.16	——	——	—	—	—	[-0.20,-0.12]	7.30	P<0.001	1.97	2.59
b_3=0.20	——	——	—	—	—	[0.18, 0.21]	28.98	P<0.001	1.97	2.59

Table S4 Statistic results for regressions in Figure 3

	Regression y=a+bx	F-value	P-value	$F_{0.05}$	$F_{0.01}$	$F_{0.001}$	Effect size (r)	F-test result
Figure 3c sample 1	b=0.73	4.47	0.04	3.93	6.88	11.44	0.37	*
Figure 3C sample 2	b=1.31	5.89	0.02	4.08	7.30	12.56	0.35	*
Figure 3C sample 3	b=15.17	17.63	P<0.001	4.54	8.68	16.59	0.74	***
Figure 3C sample 4	b=3.40	5.12	0.04	4.60	8.86	17.14	0.52	*
Figure 3C sample 5	b=7.54	11.37	0.002	4.13	7.44	12.97	0.52	**

*-significant, $0.01<p\leq0.05$
**-very significant, $0.001<p\leq0.01$
***-extremely significant, $p\leq0.001$

Table S5 Statistic results for parameters of regressions in Figure 3

	Regression y=a+bx	T-value	P-value	$T_{0.05}$	$T_{0.01}$	$T_{0.001}$	95% confidence interval	T-test result
Figure 3c sample 1	b=0.73	2.11	0.04	1.98	2.62	3.38	[0.06, 1.43]	*
Figure 3C sample 2	b=1.31	2.43	0.02	2.02	2.70	3.54	[0.22, 2.40]	*
Figure 3C sample 3	b=15.17	4.20	P<0.001	2.13	2.95	4.07	[7.47, 22.87]	***
Figure 3C sample 4	b=3.40	2.26	0.04	2.14	2.98	4.14	[0.18, 6.62]	*
Figure 3C sample 5	b=7.54	3.37	0.002	2.03	2.73	3.60	[2.99, 12.08]	**

*-significant, $0.01<p\leq0.05$
**-very significant, $0.001<p\leq0.01$
***-extremely significant, $p\leq0.001$

Table S6. Forward speed and rotational/beating frequency of sperms

Species	Rotational/beating frequency of tail (Hz)	Forward speed (μm/s)	Ratio (μm)
Bull[5]	23	126	5.5
Human[6]	~	~	1.37
Paddlefish[7]	50	175	3.5
Shovelnose sturgeon[7]	48	200	4.17
Sterlet[8]	52	160~200	3.07~3.85
Ray	**6.2**	**91.9**	**14.8**

Table S7 Statistic results for regressions in Figure 4

	Regression y=a+bx	F-value	P-value	$F_{0.05}$	$F_{0.01}$	$F_{0.001}$	Effect size (r)	F-test result
Figure 4E sample 1	b=0.12	4.13	0.04	3.86	6.69	10.96	0.18	*
Figure 4E sample 2	b=0.02	6.58	0.01	3.87	6.70	11.00	0.16	*
Figure 4E sample 3	b=0.25	6.52	0.01	3.89	6.76	11.14	0.20	*
Figure 4E sample 4	b=0.17	4.28	0.04	3.86	6.69	10.96	0.14	*
Figure 4E sample 5	b=0.08	4.38	0.04	3.86	6.69	10.96	0.14	*
Figure 4E sample 6	b=0.09	5.40	0.02	3.86	6.69	10.96	0.16	*

*-significant, $0.01<p\leq0.05$
**-very significant, $0.001<p\leq0.01$
***-extremely significant, $p\leq0.001$

Table S8 Statistic results for parameters of regressions in Figure 4

	Regression y=a+bx	T-value	P-value	$T_{0.05}$	$T_{0.01}$	$T_{0.001}$	95% confidence intervals	T-test result
Figure 4E sample 1	b=0.12	2.03	0.04	1.96	2.59	3.31	[0.02, 0.23]	*
Figure 4E sample 2	b=0.02	2.56	0.01	1.97	2.59	3.32	[0.003, 0.03]	*
Figure 4E sample 3	b=0.25	2.55	0.01	1.97	2.60	3.34	[0.12, 0.39]	*
Figure 4E sample 4	b=0.17	2.07	0.04	1.96	2.59	3.31	[0.05, 0.30]	*
Figure 4E sample 5	b=0.08	2.09	0.04	1.96	2.59	3.31	[0.03, 0.13]	*
Figure 4E sample 6	b=0.09	2.32	0.02	1.96	2.59	3.31	[0.02, 0.16]	*

*-significant, $0.01<p\leq0.05$
**-very significant, $0.001<p\leq0.01$
***-extremely significant, $p\leq0.001$

Table S9 Viscosity of solutions

Solution	Normal solution	+0.1% alginate	+0.2% alginate	+0.3% alginate	+0.4% alginate
Viscosity (mPa·s)	4	5.6	17.6	28	77
Solution	+0.5% alginate	+0.6% alginate	+0.8% alginate	+1.0% alginate	+1.5% alginate
Viscosity (mPa·s)	95	137	168	216	496

Table S10. Parameters for the calculation of the Reynolds number

	ρ (kg/m^3)	v (μm/s)	l (μm)	μ (mPa · s)	Re
Sperm in normal solution	1053	90	118	4	2.8×10^{-3}
Sperm in viscous solution i	1103	66	118	95	9.0×10^{-5}
Sperm in viscous solution ii	1155	68	118	216	4.3×10^{-5}
Sperm in viscous solution iii	1205	39	118	496	1.1×10^{-5}
Robot in silicon oil solution	963	674~1873	10902	800	8.8×10^{-3}~24.6×10^{-3}

Table S11 Statistic results for regressions in Figure 5H

	Regression y=a+bx	F-value	P-value	$F_{0.05}$	$F_{0.01}$	$F_{0.001}$	Size effect (r)	F-test result
Figure 5H VS i-1	b=0.68	12.79	P<0.001	3.88	6.73	11.09	0.22	***
Figure 5H VS i-2	b=0.16	6.21	0.01	3.86	6.69	10.96	0.18	*
Figure 5H VS i-3	b=0.23	4.56	0.03	3.86	6.69	10.96	0.22	*
Figure 5H VS ii-1	b=0.25	7.05	0.008	3.86	6.69	10.96	0.12	**
Figure 5H VS ii-2	b=0.34	7.05	0.008	3.86	6.74	11.09	0.23	**
Figure 5H VS ii-3	b=0.18	4.02	0.045	3.86	6.69	10.96	0.12	*
Figure 5H VS iii-1	b=0.46	4.90	0.03	3.96	6.96	11.67	0.24	*
Figure 5H VS iii-2	b=0.33	8.17	0.005	3.94	6.91	11.53	0.28	**
Figure 5H VS iii-3	b=1.08	12.47	P<0.001	3.96	6.96	11.67	0.37	***

*-significant, $0.01<p\leq0.05$
**-very significant, $0.001<p\leq0.01$
***-extremely significant, $p\leq0.001$

Table S12 Statistic results for parameters of regressions in Figure 5

	Regression y=a+bx	T-value	P-value	$T_{0.05}$	$T_{0.01}$	$T_{0.001}$	95% confidence interval	T-test result
Figure 5H VS i-1	b=0.68	3.58	P<0.001	1.96	2.60	3.33	[0.31, 1.06]	***
Figure 5H VS i-2	b=0.16	2.49	0.01	1.96	2.59	3.31	[0.03, 0.28]	*
Figure 5H VS i-3	b=0.23	2.14	0.03	1.96	2.59	3.31	[0.02, 0.45]	*
Figure 5H VS ii-1	b=0.25	2.66	0.008	1.96	2.59	3.31	[0.06, 0.43]	**
Figure 5H VS ii-2	b=0.34	2.66	0.008	1.96	2.60	3.33	[0.09, 0.59]	**
Figure 5H VS ii-3	b=0.18	2.01	0.045	1.96	2.59	3.31	[0.004, 0.35]	*
Figure 5H VS iii-1	b=0.46	2.21	0.03	1.99	2.64	3.41	[0.05, 0.87]	*
Figure 5H VS iii-2	b=0.33	2.86	0.005	1.99	2.63	3.40	[0.10, 0.56]	**
Figure 5H VS iii-3	b=1.08	3.53	P<0.001	1.99	2.64	3.42	[0.47, 1.69]	***

*-significant, $0.01<p\leq0.05$
**-very significant, $0.001<p\leq0.01$
***-extremely significant, $p\leq0.001$

Table S13 Statistic results for regressions in 7 viscous solutions.

	Regression Y=a+bx (95% confidence interval)	F-value	P-value	$F_{0.05}$	$F_{0.001}$	Effect size (r)	F-test result	T-value	P-value	$T_{0.05}$	$T_{0.001}$	T-test result
0.1% alginate-1	b =0.27 [0.01, 0.52]	4.38	0.04	3.95	11.57	0.24	*	2.09	0.04	1.99	3.40	*
0.1% alginate-2	b =0.66 [0.11, 1.21]	5.69	0.02	3.94	11.53	0.25	*	2.38	0.02	1.99	3.40	*
0.2% alginate-1	b =0.43 [0.08, 0.79]	6.05	0.02	3.94	11.52	0.24	*	2.46	0.02	1.99	3.40	*
0.2% alginate-2	b =0.58 [0.02, 1.14]	4.23	0.04	3.96	11.68	0.23	*	2.06	0.04	1.99	3.42	*
0.3% alginate-1	b =0.50 [0.06, 0.94]	5.07	0.03	3.94	11.53	0.23	*	2.25	0.03	1.99	3.40	*
0.3% alginate-2	b =0.55 [0.33, 0.76]	25.30	<0.001	3.94	11.52	0.45	***	5.03	<0.001	1.99	3.40	***
0.4% alginate-1	b =0.51 [0.03, 0.99]	4.44	0.04	3.94	11.52	0.21	*	2.11	0.04	1.99	3.40	*
0.4% alginate-2	b =0.19 [0.008, 0.37]	4.30	0.04	3.94	11.53	0.22	*	2.07	0.04	1.99	3.40	*
0.6% alginate-1	b =0.28 [0.02, 0.53]	4.56	0.04	3.94	11.53	0.21	*	2.13	0.04	1.99	3.40	*
0.6% alginate-2	b =0.63 [0.03, 1.22]	4.40	0.04	3.95	11.53	0.22	*	2.10	0.04	1.99	3.40	*
0.8% alginate-1	b =0.42 [0.06, 0.78]	5.32	0.02	3.97	11.72	0.26	*	2.30	0.02	1.99	3.42	*
0.8% alginate-2	b =0.41 [0.05, 0.77]	5.05	0.03	3.96	11.65	0.26	*	2.25	0.03	1.99	3.41	*

*-significant, $0.01<p\leq0.05$
**-very significant, $0.001<p\leq0.01$
***-extremely significant, $p\leq0.001$

Table S14. Motility of sperms in viscous solutions

Species	Viscosity of dilute solution (mPa·s)	Velocity in dilute solution (μm/s)	Viscosity of viscous solution (mPa·s)	Velocity in viscous solution (μm/s)	Velocity decrease ratio
Bull[9]	0.7	200	22.6	75	62.5%
Human[9]	1	53.5	20	29.7	44%
Human[10]	20	~	250	~	43%
Ray	**4**	**91.9**	**216**	**68**	**26%**

Table S15. Parameters for estimating the drag force from the midpiece of the robot.

Viscosity (mPa·s)	C_D	ρ (kg/m^3)	U (mm/s)	l (mm)	D (mm)	F (N)
100	9.43	963	7.77	8	4	8.77×10^{-6}
200	9.43	963	4.27	8	4	2.65×10^{-6}
400	9.43	963	2.35	8	4	8.02×10^{-7}
800	9.43	963	0.67~1.87	8	4	6.5×10^{-8}~5.08×10^{-7}
1600	9.43	963	0.76	8	4	8.39×10^{-8}

Table S16. The detailed data for the dual/single helical driven robot.

Viscosity (mPa·s)	Dual helix (mm/s)	Helical tail (mm/s)	Ratio	Helical head (mm/s)	Ratio
100	7.73257	4.61646	1.675	2.91457	2.653
200	4.26859	2.38357	1.791	1.49841	2.849
400	2.35412	1.41487	1.667	1.30918	1.798
800	1.3913	0.65511	2.124	0.87299	1.595
1600	0.76245	0.17129	4.451	0.47246	1.614

Movie S1 (separate file)

The heter-stiffness helical morphology of the Ray sperm. The video shows the heter-stiffness helical morphology of Ray sperms under an optical microscope, scanning electron microscope, and confocal microscope.

Movie S2 (separate file)

The heter-stiffness helical propulsion of the Ray sperm. This video shows the 3D rotational motion of both the spiral head and helical tail. The head and tail rotates counter-clockwise to the forward direction, and both propels the body.

Movie S3 (separate file)

Bi-directional motions of Ray sperms. The sperm (sample 1) first moves backward with the head rotating. Then, it is in a state of transition, with the change of the rotational direction. Finally, it moves forward with both head and tail rotation. For sample 2, the sperm first moves backward to avoid the obstacle. After escaping from the obstacle, it moves forward.

Movie S4 (separate file)

Environmental adaptability of Ray sperms. This video shows the motility of Ray sperms in the normal solution, viscous solution i, viscous solution ii, and viscous solution iii. In the normal solution, the Ray sperms move forward with dual helical propulsion. In viscous solutions, although the tails twine as circles, the sperms still can move forward with the propulsion from the head.

Movie S5 (separate file)

Motions of the bio-inspired robot in various viscous solutions. First, the robot is driven by a single spiral head or helical tail with the same power input in solutions with increasing viscosities (Figs. S25-S26). In the diluted solution, the robot driven by a single tail moves faster. On the contrary, the robot with a single head is more efficient in highly viscous solutions. Then, the video displays the performance of robots with single or dual helical driven mode. The robot is driven by heter-stiffness helical morphology, single spiral head, or single helical tail with the same power input in different solutions. The robot with heter-stiffness helical sections moves fastest in all solutions. The robot with a single helical head or tail relatively adapts to the viscous and diluted solution, respectively.

Code availability

Matlab was used to generate custom-written scripts to analyze the motility parameters, fit the shape of the sperm, calculate the propulsive force, and fit the relationship between the rotational speed and the moving velocity.

1. Calculation of the mobility parameters

```
%% Opening the Video

vidObj = VideoReader('Ray 4.mp4');
video = read(vidObj,1);
cc = (rgb2gray(video));
k = 1;
framesn = vidObj.NumberOfFrames;
P =[];

for k = 1:5:framesn
    A =  (read(vidObj,k));
   imshow(A);
   P(k,:) = ginput(1);
end
 %%
```

```
 Po = [P(:,1) P(:,2)];
xlswrite('Ray 4',Po);
%%
Po = xlsread('Ray 4.xls');
Pp = unique(Po,'rows');
%i = 1:4:200
%Pp = Pp(i,:);
%% Plotting the Data obtained from video to measure VCL, VAP & VSL:
Po= [Pp(:,1) Pp(:,2)];
%494
%Po = Pt;
%Po(1:4,:)=[];%remove 1 to 4 points
long = length(Po);
FR = 200.00;% frames/sec
Apparatus = 0.33;% um/pixel
Dframes = norm(Po(1,:)-Po(end,:));%distance in pixels between 10 consectuive frames
Davg = Dframes/(long-1)% Average distance in pixels per frame
Vframe = Davg*FR;% velocity pixels/sec
SpeedVSL = Vframe*Apparatus% um/sec
%VCL
Dframes = [];Df = [];
for i = 1: long-1
Dframes(i) = norm(Po(i,:)-Po(i+1,:));%distance in pixels between 10 consectuive frames
%Df = Dframes+Df;
end
Davg = sum(Dframes)/(long-1);% Average distance in pixels per frame
Vframe = Davg*FR;% velocity pixels/sec
SpeedVCL = Vframe*Apparatus;% um/sec

x = Po(:,1);
y = Po(:,2);
p = polyfit(x,y,4);
xn = min(x):0.01:max(x);
f = polyval(p,xn);

pt = interparc(500,x,y,'spline');
 %Plot the result
%AL = arclength(xn,f,'s');% l,p,s
CLF = hypot(diff(xn),diff(f));
CL = trapz(CLF);
%
Davg = CL/(long-1);% Average distance in pixels per frame
Vframe = Davg*FR;% velocity pixels/sec
SpeedVAP = Vframe*Apparatus;% um/sec

scatter(Po(:,1),Po(:,2),'k*');hold on%original data
plot(pt(:,1),pt(:,2),'c-','linewidth',2);%interpolanted
plot(Po(:,1),Po(:,2),'r-','linewidth',2);hold on%vcl
plot(xn,f,'b-','linewidth',2);%vap
plot([Po(1,1) Po(end,1)],[Po(1,2) Po(end,2)],'g-','linewidth',2)%vsl
legend('original','Interpolated','VCL ','VAP','VSL');

legend(['Original'],['Interpolated'],['VCL = ' num2str(SpeedVCL)],['VAP = '
num2str(SpeedVAP)],['VSL = ' num2str(SpeedVSL) ]);

%title(['VCL=' num2str(SpeedVCL) '   VAP=' num2str(SpeedVAP) '   VSL=' num2str(SpeedVSL) ]);
```

```
title('Tracking parameters');
%grid on
 xlim([250 500]);
 ylim([400 500]);
%set(gca,'Ydir','reverse');
%% Saving the results into VCL/VAP/VSL:
saveas (gcf,[num2str(2) 'Ray 4.png']);
% final results
SpeedVCL;
SpeedVAP;
SpeedVSL;
LIN = (SpeedVSL/SpeedVCL)*100;
STR = (SpeedVSL/SpeedVAP)*100;
WOB = (SpeedVAP/SpeedVCL)*100;
%
LastName = {'SpeedVCL';'SpeedVAP';'SpeedVSL';'LIN';'STR';'WOB'};
Values = [SpeedVCL; SpeedVAP; SpeedVSL ;LIN; STR; WOB];

T = table(Values,...
    'RowNames',LastName)
%
2. Calculation of the propulsive force
load('fittedshape20181203_v2.mat');%contain the fitted data
load('plotshape20181128.mat');%contain the plot shape data
%%
%%
L=z_all(1,end)*10^(-6);%
global x1 x2 x3
x1=z_head(end)*10^(-6);%end of the head
x2=z_mid(end)*10^(-6);%end of the midpiece
x3=z_all(end)*10^(-6);%length of the total body
%%
k=size(rv_head,1);
global U omega
for i=1:k
omega=[rv_head(i),rv_tail(i)];%rotation speed
U=fv(i)*10^(-6);% forward velocityspeed
y0=zeros(1,2);
[simx1,f1] = ode45(@thrust_body_head,[0:1*10^-8:x1],y0);
[simx2,f2] = ode45(@thrust_body_head,[x1:1*10^-8:x2],y0);
[simx3,f3] = ode45(@thrust_body_head,[x2:1*10^-8:x3],y0);
fpro_head(:,i)=f1(:,1);flat_head(:,i)=f1(:,2);
simx_head(:,i)=simx1(:,1);
fpro_mid(:,i)=f2(:,1);flat_mid(:,i)=f2(:,2);
simx_mid(:,i)=simx2(:,1);
fpro_tail(:,i)=f3(:,1);flat_tail(:,i)=f3(:,2);
simx_tail(:,i)=simx3(:,1);
ratio_head(i)=f1(end,1)/(f1(end,1)+f2(end,1)+f3(end,1))*100;
ratio_tail(i)=f3(end,1)/(f1(end,1)+f2(end,1)+f3(end,1))*100;
end
meanhead=mean(ratio_head);stdhead=std(ratio_head);
meantail=mean(ratio_tail);stdtail=std(ratio_tail);
%%
subplot(1,2,1)
plot([1:k],ratio_head,[1:k],ratio_tail)
subplot(1,2,2)
```

```
plot(simx1,f1(:,1),simx3,f3(:,1)+f1(end,1))

%
function dy=thrust_body_head(xs,y)
load('fittedshape20181203_v2.mat');%contain the fitted data
load('plotshape20181128.mat');%contain the plot shape data
global U omega x1 x2 x3
mu=4*10^-3;%
if xs<=x1
   sitathr=fittedmodel_sita_head(xs*10^(6));%
   lamda=fittedmodel_hw_head(sitathr)*2*10^(-6);%the unit of lamda is m
   A=fittedmodel_am_head(sitathr)*10^(-6);
end
if (xs>x1)&&(xs<=x2)
   lamda=10^-5;
   A=10^-8;
   sitathr=0;
end
if (xs>x2)&&(xs<=x3)
   sitathr=fittedmodel_sita_tail(xs*10^(6)-x2*10^(6));
   lamda=fittedmodel_hw_tail(sitathr)*2*10^(-6);
   A=fittedmodel_am_tail(sitathr)*10^(-6);
end
L=lamda;
a=(8.35*10^-3*xs+0.57)*10^(-6);%
phi=atan(lamda/(2*pi*A));
psita=pi/2-phi;
%%
%
q1=L;
ct=zeros(1,5);
cn=zeros(1,5);
% for i=1:N
ct(1)=2*pi*mu/(log(2*q1/a)-0.5);
cn(1)=4*pi*mu/(log(2*q1/a)+0.5);
dft=zeros(1,5);
dfn=zeros(1,5);
for k=1:1%
%     for  i=1:N
   if (xs<=x1)%head
      dft(k)=ct(k)*(U*sin(phi)+omega(1)*A*cos(phi));
      dfn(k)=cn(k)*(omega(1)*A*sin(phi)-U*cos(phi));
      dfx(k)=(dfn(k)*sin(psita)-dft(k)*cos(psita))/sin(phi);
   end
   if (xs>x1)&&(xs<=x2)%midpiece
      dft(k)=ct(k)*(0*sin(phi)+omega(1)*0*cos(phi));
      dfn(k)=cn(k)*(omega(1)*0*sin(phi)-0*cos(phi));
      dfx(k)=(dfn(k)*sin(psita)-dft(k)*cos(psita))/sin(phi);
   end
   if (xs>x2)&&(xs<=x3)%tail
      dft(k)=ct(k)*(U*sin(phi)+omega(2)*A*cos(phi));
      dfn(k)=cn(k)*(omega(2)*A*sin(phi)-U*cos(phi));
      dfx(k)=(dfn(k)*sin(psita)-dft(k)*cos(psita))/sin(phi);
   end
dy=zeros(1,1);
dy(1)=dfx(1);
```

References

1. K. Andraszek, D. Banaszewska, B. Biesiada-Drzazga, The use of two staining methods for identification of spermatozoon structure in roosters. *Poultry science* **97**, 2575-2581 (2018).
2. S. H. Alavi, M. Rodina, A. T. Viveiros, J. Cosson, D. Gela, S. Boryshpolets, O. Linhart, Effects of osmolality on sperm morphology, motility and flagellar wave parameters in Northern pike (Esox lucius L.). *Theriogenology* **72**, 32-43 (2009).
3. M. Psenicka, S. H. Alavi, M. Rodina, D. Gela, J. Nebesarova, O. Linhart, Morphology and ultrastructure of Siberian sturgeon (Acipenser baerii) spermatozoa using scanning and transmission electron microscopy. *Biology of the Cell* **99**, 103-115 (2007).
4. Z. Linhartova, M. Rodina, J. Nebesarova, J. Cosson, M. Psenicka, Morphology and ultrastructure of beluga (Huso huso) spermatozoa and a comparison with related sturgeons.
5. M. Wilson, J. Harvey, P. Shannon, Aerobic and anaerobic swimming speeds of spermatozoa investigated by twin beam laser velocimetry. *Biophysical journal* **51**, 509-512 (1987).
6. E. Subramani, H. Basu, S. Thangaraju, S. Dandekar, D. Mathur, K. Chaudhury, Rotational dynamics of optically trapped human spermatozoa. *The Scientific World Journal* **2014**, (2014).
7. J. Cosson, O. Linhart, S. Mims, W. Shelton, M. Rodina, Analysis of motility parameters from paddlefish and shovelnose sturgeon spermatozoa. *Journal of Fish Biology* **56**, 1348-1367 (2000).
8. S. Boryshpolets, J. Cosson, V. Bondarenko, E. Gillies, M. Rodina, B. Dzyuba, O. Linhart, Different swimming behaviors of sterlet (Acipenser ruthenus) spermatozoa close to solid and free surfaces. *Theriogenology* **79**, 81-86 (2013).
9. V. Kantsler, J. Dunkel, M. Blayney, R. E. Goldstein, Rheotaxis facilitates upstream navigation of mammalian sperm cells. *Elife* **3**, e02403 (2014).
10. L. Eamer, R. Nosrati, M. Vollmer, A. Zini, D. Sinton, Microfluidic assessment of swimming media for motility-based sperm selection. *Biomicrofluidics* **9**, 044113 (2015).